Non-Destructive Estimation of Leaf Area Index(LAI) Using Image Data

A thesis submitted to the
College of Graduate and Postdoctoral Studies
in partial fulfillment of the requirements
for the degree of Master of Science
in the Department of Mechanical Engineering
University of Saskatchewan
Saskatoon

By
Tansu SEDIQI

Permission to Use

In presenting this thesis in partial fulfillment of the requirements for a Postgraduate degree from the University of Saskatchewan, I agree that the Libraries of this University may make it freely available for inspection. I further agree that permission for copying of this thesis in any manner, in whole or in part, for scholarly purposes may be granted by the professor or professors who supervised my thesis work or, in their absence, by the Head of the Department or the Dean of the College in which my thesis work was done. It is understood that any copying or publication or use of this thesis or parts thereof for financial gain shall not be allowed without my written permission. It is also understood that due recognition shall be given to me and to the University of Saskatchewan in any scholarly use which may be made of any material in my thesis.
Requests for permission to copy or to make other uses of materials in this thesis in whole or part should be addressed to:

Head of the Department of Mechanical Engineering
3B48 Engineering Building
57 Campus Drive University of Saskatchewan
Saskatoon, Saskatchewan
Canada
S7N 5A9

OR

Dean
College of Graduate and Postdoctoral Studies
University of Saskatchewan
116 Thorvaldson Building, 110 Science Place
Saskatoon, Saskatchewan S7N 5C9 Canada

Disclaimer

Reference in this thesis to any specific commercial products, process, or service by trade name, trademark, manufacturer, or otherwise, does not constitute or imply its endorsement, recommendation, or favoring by the University of Saskatchewan. The views and opinions of the author expressed herein do not state or reflect those of the University of Saskatchewan, and shall not be used for advertising or product endorsement purposes.

Abstract

This study investigated using image data to estimate the Leaf Area Index (LAI) for wheat (*Triticale aestivum* L.). The calculation of LAI involved the utilization of light interception, and the estimation process involves creating a model using metrics extracted from Near-Infrared (NIR) and visible light image data.

Line quantum sensors were used to collect above- and below-canopy light measurements. Standard models were used to calculate LAI based on these measurements. To address the effects of the sun azimuth angle, corrections were applied to the LAI values, effectively eliminating its impact on the determinations.

The assessment of canopy coverage used in this study involved NIR and visible light images. To estimate LAI non-destructively, linear regression models were constructed, incorporating a set of metrics from the mentioned imaging modalities and the date as a proxy for the maturity of the wheat canopy.

The performance of these models was evaluated using root mean squared error (RMSE) and adjusted coefficient of determination (R^2). Through a comparison of these models, it was concluded that LAI was best estimated using NIR images, rather than visible-light images. Moreover, the most effective model for the estimation of LAI included only canopy coverage and maturity proxy as input parameters. Height was not an important factor in this case.

The dataset examined contained a set of wheat varieties. To improve the power of LAI estimation models, the study employed a clustering technique. Rather than using a single, generic model for LAI estimation across all varieties, the proposed clustering strategy involves clustering the dataset and developing a model for each distinct cluster. This departure from the one-size-fits-all approach generated more precise LAI estimations for each cluster, ultimately enhancing the overall predictive accuracy of the models. This not only enhanced comprehension of LAI dynamics but also underscored the significance of personalized strategies in agricultural research to achieve more precise and applicable results. However, there are certain limitations to consider. The clusters showed inconsistencies, indicating possible difficulties in putting them into practice. While the suggestion of clustering exists, the specific approach to resolving these inconsistencies remains uncertain.

Acknowledgements

I would like to express my sincere gratitude to Dr. Scott Noble, my advisor, for his invaluable guidance, consistent support, and insightful input during the entire thesis process. Dr. Noble's expertise and dedication have significantly influenced the direction and quality of this research.

I want to convey my gratitude to Dr. Raju Soolanayakanahally and Subarna Sharma from Agriculture and Agri-Food Canada (AAFC) for graciously allowing us to utilize their plots, and their invaluable help has significantly enhanced the study.

Additionally, I would like to acknowledge the Saskatchewan Wheat Development Commission (Sask Wheat), the Western Grains Research Foundation (WGRF), and the Plant Phenotyping and Imaging Research Centre (P^2IRC) for their financial support, which has been instrumental in the execution of this research.

I also want to express my thanks to all individuals, colleagues, and friends who have played various roles in supporting this research, especially extending appreciation to Keith Halcro and Tyrone Keep for their valuable contributions to collecting data. Additionally, I extend my gratitude to the committee members for their insightful feedback and guidance. Your efforts, alongside theirs, have been invaluable, enhancing the overall quality and depth of this thesis.

In conclusion, the completion of this thesis would not have been possible without the guidance and contributions of these individuals and organizations. I appreciate the encouragement, assistance, and collective efforts that have shaped this academic journey. Thank you for your ongoing support.

I dedicate this thesis to my son, who fills my life with joy, and to my newly born daughter, who has just joined our family. Your presence motivates my dedication to academic pursuits. This work symbolizes my commitment to ensuring a promising future for both of you. As I navigate the challenges of parenthood, I anticipate sharing the insights gained during this academic journey with you both.

Contents

List of Tables

List of Figures

List of Abbreviations

3D	3-Dimensional
AAFC	Agriculture and Agri-Food Canada
ANN	Artificial Neural Network
GAM	Generalized Additive Model
GDD	Growing Degree Day
LAI	Leaf Area Index
LAI_{AZ}	LAI values derived from the PAR readings with azimuth angle correction
LAI_{GAM}	LAI values predicted by GAM
LAI_{MODEL}	LAI values predicted by model
LAI_{PAR}	LAI values derived from the PAR readings
LUT	Look-up Table
NIR	Near-Infrared
P^2IRC	Plant Phenotyping and Imaging Research Centre
PAI	Plant Area Index
PAR	Photosynthetically Active Radiation
R^2	R-squared, Coefficient of Determination
RGB	Red, Green, and Blue
RMSE	Root Mean Squared Error
SVMR	Support Vector Machines Regression
SWIR	Shortwave Infrared
TOF	Time-of-Flight
UFPS	USASK Field Phenotyping System
VIs	Vegetation Indices
WGRF	Western Grains Research Foundation

1 Introduction

Leaf area index (LAI) is a measure of the amount of leaf material within a canopy (Bollinger, 2023). The extraction of LAI is important for many studies of plant physiology, ecology, and breeding. LAI is the total one-sided area of leaves per unit ground area (Chen and Black, 1992). This metric serves as a proxy for a plant canopy's growth and yield potential as well as its overall performance (Roth et al., 2018). Leaves are a critical interface between the plant and the environment. Consequently, LAI finds application in a wide range of fields such as agriculture, ecology, and forests (Mananze et al., 2018). LAI can be an indicator of water stress, biomass, crop growth stage (Raj et al., 2021), microclimate change below the canopy, sunlight interception, water exchange, and gas exchange (Bréda, 2003).

The insights offered by LAI are valuable to ecophysiologists, ecologists, etc. However, quantifying canopy LAI is difficult because of its spatial and temporal changes. These changes could be caused by annual cycles, variability between years, and heterogeneity (Bréda, 2003). Yang et al. (2007) observed temporal changes in LAI throughout the growth stages of winter wheat (*Triticale aestivum* L.), recognizing that factors such as water status, field management, and soil conditions played a significant role in inducing spatial variations in LAI. To comprehend crop growth and development, tracking the spatial and temporal variation of LAI with varying environments, growth stages, and agronomic treatments is essential (Yang et al., 2007). Replicates at multiple locations should always be used to determine LAI because of the high spatial variability found in canopies, which makes sampling highly important. The key to improving LAI measurement might be precisely identifying the variables that influence its variability. It is essential, for example, to comprehend the extent to which a single leaf area varies over successive years or between locations. (Bréda, 2003).

There are several approaches and methods for measuring LAI. Approaches can be categorized as direct and indirect methods. Direct methods measure the representative leaf samples and can only be applied to small areas due to the effort required (Behera et al., 2010). Direct methods measure LAI by harvesting and applying gravimetric or planimetric techniques to calculate LAI. Prior knowledge of green leaf area and leaf dry weight ratio are used to find the correlation between leaf dry weight and LAI for estimating LAI with the gravimetric technique. The planimetric technique compares the total leaf area to the ground area and is the definition of LAI (Aschonitis et al., 2014). Indirect methods are non-destructive and measure various interactions of light with the plant canopy as measured by optical instruments (Behera et al., 2010). These include spectrometers, LiDAR, and measurements of light interception by the canopy.

Within this research, one of the key objectives was to estimate LAI in a non-destructive manner. Alongside this primary aim, the study also sought to explore various factors that may impact LAI estimation, which

had potentially been overlooked by existing methods. Particular attention was given to investigating the influence of the sun's azimuth angle on LAI calculations using line quantum sensor measurements.

In this study, a non-destructive approach was adopted, employing correlation between canopy coverage and LAI as a method to assess LAI. To evaluate the effectiveness of LAI estimation, a comparative analysis was conducted between canopy coverage calculated from visible light images and that derived from near-infrared (NIR) images. This comparison aimed to provide insights into the accuracy and reliability of LAI estimation through different imaging modalities.

To achieve non-destructive LAI estimation, various models were developed, each showcasing distinct input metrics. These metrics included canopy coverage derived from NIR and visible light images, along with maturity proxies, all aimed at identifying the most effective approaches. Additionally, some models did not incorporate the entire dataset to understand the impact of partial data on model performance, achieved by removing specific varieties from the dataset. Furthermore, diverse models were created for different clusters of varieties. Investigation of the influence of clustering on the success rate of LAI estimation was achieved with these diverse models.

2 Literature Review

The leaf area index (LAI) can be used in evaluating genetic variability among different genotypes. Gerrano et al. (2015) underscore the utility of LAI as a valuable metric for evaluating genetic distances among genotypes (Gerrano et al., 2015). Battaglia et al. (1998) showed the gradual reduction in LAI under water stress, along with species-specific variations in response to growth temperatures, highlighting the sensitivity of LAI to subtle changes in experimental conditions (Battaglia et al., 1998). The LAI value for a wheat canopy typically falls within the range of 0.5 to 5 (Afrasiabian et al., 2021; Chattaraj et al., 2011; Rahman et al., 2014).

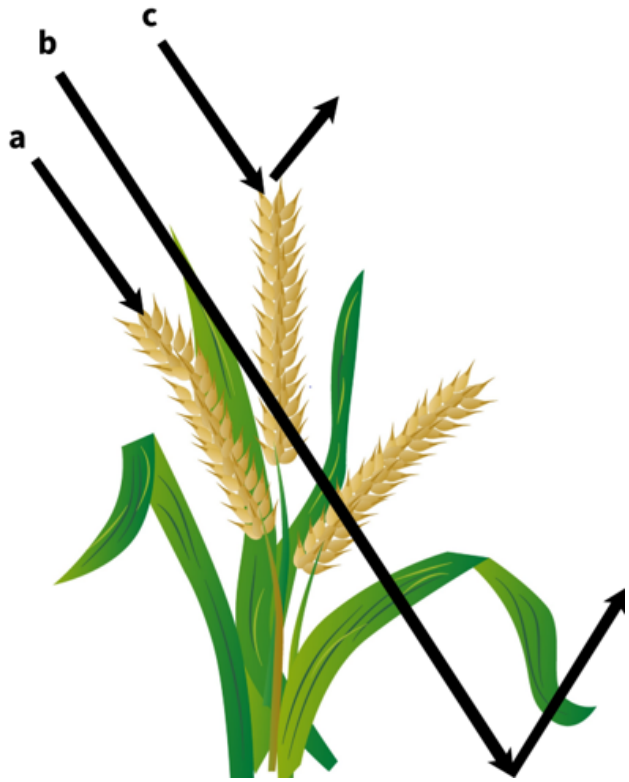

Figure 2.1: Canopy-light interaction. Light can be (a) absorbed by the canopy, (b) transmitted through the canopy and absorbed or reflected at the soil surface, or (c) reflected by the canopy itself.

Light interacts with the canopy in different ways as shown in Figure 2.1. Efficient light harvesting in ecosystems involves dynamic adjustments at the leaf, plant, and canopy levels. Variations in chlorophyll content and leaf dry mass per unit area impact light interception at the leaf level (Zhang et al., 2005; Rosati,

2001). Shoot-level factors, such as foliage inclination and spatial arrangement, play a pivotal role, while at the canopy level branching frequency and foliage distribution have significant effects on light harvesting. Plastic modifications in traits, like chlorophyll per mass, enable plants to adapt to varying light conditions. Shade-tolerant species exhibit specific traits, including extended leaf longevity. Changes in foliage aggregation due to plant age and size influence light harvesting efficiency during development (Fleck et al., 2003; Niinemets, 2010). In summary, the effectiveness of light harvesting in plants is determined by a combination of adaptable chemical and architectural traits across different scales (Niinemets, 2010).

The quantity of light intercepted by crops throughout the growing season influences their growth (Monteith and Moss, 1977). Photosynthetically active radiation (PAR) light interception, and therefore yield, are affected by the leaf area (Stewart et al., 2003). Although the significance of light interception is widely acknowledged, it is often neglected due to the challenge of measuring it (Purcell, 2000). LAI can be used as an alternative to measuring how much light the canopy absorbs (Li et al., 2019). The light interception grows quickly as LAI increases (Firman and Allen, 1989).

Several field investigations have documented how variations in the angle of the sun can influence how light is reflected from the canopy. To obtain precise measurements of light interception, it is important to take into account significant factors like row spacing and time of day (Flénet et al., 1996). Ranson et al. (1985) concluded that the positioning of the sensor relative to the sun significantly influences the light reflected from canopies (Ranson et al., 1985). The impact of the angle between the sun azimuth and the row orientation on measurements has been widely neglected. The timing of data gathering and the angle of the sun's azimuth could introduce bias in the calculation of the LAI (Salter et al., 2018).

2.1 Methods for Measuring LAI

Diverse methods are utilized to estimate LAI, each offering unique advantages and considerations. Conventional methods for estimating LAI directly, such as destructive sampling, are accurate but demand significant labor, time, and expenses (Peduzzi et al., 2012). Harvesting is a direct method for measuring LAI, which involves measuring the area of all leaves. However, this method is destructive and applicable only to small-scale sampling (Purcell, 2000).

Canopy reflectance model inversion is an indirect and non-destructive approach. These models are bidirectional (Liu et al., 2016). The most used model is the PROSAIL model which is a combination of the PROSPECT leaf optical properties model and the SAIL canopy radiative transfer model. Coupling of these models takes place using leaf reflectance and transmittance which are an output of the PROSPECT model, as inputs to the SAIL model (Berger et al., 2018). PROSAIL is the most used canopy optical property model because of its robustness, consistent validation results, and simplicity. It is available in several computer languages for free (Jacquemoud et al., 2009).

There are different inversion strategies for calculating LAI from canopy reflectance models (Fei et al.,

2012). The complexity of physical models makes inversion strategies necessary for LAI estimation (Liu et al., 2016). A look-up table (LUT) is one of the most used model inversion strategies. The LUT could be created through forward calculations using a model. The best fit between measured value and LUT spectra could be found by search operation, and this could be used as inversion. The LUT must be large enough to get high accuracy (Darvishzadeh et al., 2008). Other approaches for physical model inversion are using artificial neural network (ANN), support vector machines regression (SVMR), and iterative optimization.

Calculating LAI by using vegetation indices (VIs) is a simple, robust, and accurate statistical approach. VIs are designed to provide only the features that the user is interested in and minimize other effects (Jay et al., 2017). However, challenges persist with VIs. VIs have been developed utilizing either narrowband spectral data or broadband sensors. Although the underlying mathematical formulations of these VIs remain constant, their derived outcomes vary, thereby impacting their dependability in forecasting LAI (Zhao et al., 2007). An additional difficulty in estimating LAI using VIs is the saturation issue that arises when VIs show limited sensitivity to high LAI. This diminished responsiveness presents obstacles in capturing LAI variations, especially in dense canopies. It is important to acknowledge this saturation challenge during result interpretation and model application (Kang et al., 2016).

Instruments exist for non-destructive measurement of LAI. These devices measure the canopy structure attributes and PAR from above and below the canopy and calculate LAI from these measurements (LI-COR, 2021; Pokovai and Fodor, 2019). The instances of such an instrument are the canopy analyzer, ceptometer, and line quantum sensor. In the literature, the most used canopy analyzer instruments are the LAI-2000 and LAI-2200 (LI-COR Inc., Lincoln, NE, USA) while the most common ceptometers in literature are the ACCUPAR LP-80 (METER Group, Inc., Pullman, WA, USA) and SunScan (Delta- T Devices, Cambridge, UK).

The canopy analyzer determines LAI by measuring light interception both below and above the canopy at five different zenith angles. It employs data collected from both above and below the canopy to compute canopy transmittance, which is then utilized to derive the LAI (LI-COR, 2021). Canopy analyzers commonly include a sensor or array of sensors positioned on a handle or frame.

The ceptometer is employed to measure PAR both above and below the canopy, utilizing these measurements to calculate LAI (Pokovai and Fodor, 2019). Ceptometers are characterized by a setup comprising a series of linear sensors or photodiodes arranged in a specific manner. Addressing angular constraints for incoming light in ceptometers can pose a challenge. Therefore, emphasis should be placed on devising sampling patterns and defining measurement conditions (López-Lozano and Casterad, 2013).

The line quantum sensor functions as a measurement tool to quantify PAR within the canopy, diverging from the conventional approach of providing LAI values as observed in traditional canopy analyzers and ceptometers. Canopy analyzers and ceptometers are tools for the estimation of LAI on their own. The measurement of PAR using a quantum sensor positioned within the canopy takes into account both scattered and transmitted light (Decagon, 2013). Additionally, it helps to account for spatial non-uniformity (LI-COR,

Inc., 2015) but it entails the trade-off of necessitating a larger number of measurements to cover the study area. This undertaking can be demanding in terms of both time and human resources. On the other hand, the flexibility to design and customize transects or measurement grids is advantageous in accommodating the distinct features of the study area. The calculation of LAI is achievable through PAR measurements, aligning with the methodology employed by the manual provided by Decagon Devices (Decagon, 2013). PAR readings, beam fraction, and extinction coefficient are required for calculating LAI. The ratio of radiation from the sun's direct beam to radiation from all other ambient sources, such as the atmosphere or reflections off other surfaces, is known as the fraction of beam radiation (Decagon, 2013). The beam fraction (f_b) can be calculated as Equation 2.1 which is derived from data analysis conducted by Decagon Devices (Decagon, nd). r is the above-canopy PAR reading divided by the cosine of the sun zenith angle times a solar constant as shown in Equation 2.2. The solar constant is presumed to be 2550 μmol/m^2/s. The zenith angle is the measurement of the angle formed by the sun in relation to the zenith, which is the point directly overhead in the sky, perpendicular to the observer's position on the ground (Decagon, 2013). If r is 0.82 or above, it is fixed to 0.82, and if it is 0.20 or below, it is fixed to 0.20 (Decagon, nd). The extinction coefficient (K) can be calculated from Equation 2.3 where χ is the leaf angle distribution parameter and is assumed to be 0.96 for wheat and θ_i is the sun zenith angle (Decagon, 2013).

$$f_b = 1.395 + r\left(-14.43 + r\left(48.57 + r\left(-59.024 + r24.835\right)\right)\right) \tag{2.1}$$

$$r = \frac{PAR_{\text{above-canopy}}}{2550 \cdot \cos(\text{Sun Zenith Angle})} \tag{2.2}$$

$$K = \frac{\sqrt{\chi^2 + \tan^2\theta_i}}{\chi + 1.744(\chi + 1.182)^{-0.733}} \tag{2.3}$$

Equation 2.4, derived from the complete Norman-Jarvis model (Norman, 1988), can be used to retrieve LAI, where τ is the ratio of below-canopy PAR value to above-canopy PAR value, and A is defined in Equation 2.5. A is 0.86 when a, which is leaf absorptivity in the PAR, is assumed to be 0.90 by Decagon Devices in LAI sampling procedures (Decagon, 2013).

$$L = \frac{(1 - \frac{1}{2K})f_b - 1}{\ln\tau / A(1 - 0.47f_b)} \tag{2.4}$$

$$A = 0.283 + 0.785a - 0.159a^2 \tag{2.5}$$

The canopy analyzer, ceptometer, and line quantum sensor are commonly used tools for the measurement of plant area index (PAI) which includes both photosynthetic and non-photosynthetic components (like

branches). If the non-photosynthetic components are not present, PAI could be considered LAI (Darvishzadeh et al., 2008; White et al., 2000).

In the literature, there are studies that use correlations for estimating LAI. Correlation-based methods establish links between LAI and ground cover, canopy cover, and height. These varied approaches cater to different canopy sizes and precision needs for LAI estimation. The canopy coverage and height are connected to the penetration of light (Allen, 1974; Korhonen et al., 2011), and the LAI provides an alternative measure for assessing the canopy's light absorption (Li et al., 2019). The correlation between these elements underscores their interdependence. Boyd et al. (2002) observed a high correlation between LAI and ground cover (Boyd et al., 2002). Zhang et al. (2019) observed that canopy cover and height could be used to estimate LAI and these parameters are complementary (Zhang et al., 2019). Nielsen et al. (2012) found that with the increase of LAI, there is a corresponding rise in canopy cover, ultimately reaching a maximum level (Nielsen et al., 2012). However, it's noteworthy that canopy coverage can saturate, especially within dense canopies (Arumäe and Lang, 2018). All these studies showed that LAI could be estimated by correlation with a high success rate.

Images are among the data sources utilized for estimating LAI. Image data, including NIR imagery (Roth and Streit, 2018) and RGB imagery (Stewart et al., 2007; Nielsen et al., 2012), can be used to compute canopy coverage (Jarquin et al., 2018), which can be used to calculate LAI (Hsiao et al., 2009; Stewart et al., 2007; Nielsen et al., 2012). Nielsen et al. (2012) and Stewart et al. (2007) utilized images to estimate canopy coverage and established the relationship between LAI and canopy coverage. Their analysis revealed strong relationships between LAI and canopy coverage.

Spectral imaging has the potential to be employed for the estimation of LAI. Spectral imaging can be categorized into two primary techniques, namely hyperspectral imaging and multispectral imaging, based on the continuity of spectral information (Qin et al., 2013). Liu et al. (2016) reported that hyperspectral data does not increase the accuracy of retrieving LAI, but that it may decrease uncertainties associated with LAI estimation. As an example, hyperspectral data could be used for improving atmospheric correction, a task that has recently been accomplished using methods grounded in rigorous radiative transfer modeling approaches (Gao et al., 2009). Another example involves improving the accuracy of interconnected variables used as input in physical models, such as chlorophyll/water content and average leaf angle (Liu et al., 2016). On the other hand, the quality of hyperspectral data depends on the bands and the sensors. Due to their high dimensionality, the utilization of hyperspectral data may pose a challenge as it has the potential to result in overfitting of statistical models (Lee et al., 2004). Multispectral data does not have a substantial difference in LAI estimation accuracy from hyperspectral data (Liu et al., 2016) Although hyperspectral data offers a larger amount of information than multispectral data, numerous adjacent wavebands contain redundant and highly correlated information (Thenkabail et al., 2004).

Red, Green, and Blue (RGB) or color imagery is an affordable alternative to the previously mentioned spectral data sources, although it comes with restrictions. RGB data do not reflect changes inside the canopy.

Only minor changes occur at the top of the canopy. Inner canopy changes are not visible through RGB data, but they could be partly visible from the infrared spectrum (Raj et al., 2021). The explanation lies in the fact that near-infrared radiation can penetrate deeper into the canopy compared to visible light, attributed to its low absorption and high transmission properties (Jensen, 1980). As numerous VIs used NIR bands to estimate LAI, utilizing RGB data or other data types lacking NIR bands for LAI estimation through VIs is diminished (Zheng et al., 2018). Shortwave infrared (SWIR) and NIR regions contain the bands most correlated with LAI (Gong et al., 2003), thus VIs containing these bands are most often used for LAI estimations.

Beyond image data, LiDAR emerges as another valuable data source for LAI estimation. LiDAR is an active remote sensing technology that measures distances by measuring the return-trip time-of-flight of a laser signal to an object (Hosoi and Omasa, 2006; Wang and Fang, 2020). The laborious and time-consuming operation of manually measuring plant height has become a limiting factor for breeding and genetics programs (Wang et al., 2018). Digital phenotyping uses sensors and cameras to measure and collect information about physical traits. This makes collecting data easier and less prone to mistakes, which helps research studies be more effective. LiDAR is one of the sensors that can be utilized to measure plant height. LiDAR sensors are classified as active remote sensing technologies as they have the capacity to produce their energy (Purkis and Brock, 2013), and these sensors can be used to create 3-dimensional (3D) images from point clouds. The time-of-flight (TOF) measuring principle is utilized for LiDAR imaging, where depth is estimated by measuring time delays in events in light emitted from a light source (Royo and Ballesta-Garcia, 2019).

Walter et al. (2019) extracted canopy height using a percentile algorithm, by identifying the 86th percentile of the dataset, following a process of refining data to eliminate false returns (Walter et al., 2019). Jimenez-Berni et al. (2018) determined canopy height from LiDAR data by generating a histogram representing distances relative to the LiDAR, determining the peak of the histogram as the ground height, and subsequently estimating canopy height as the difference between the ground elevation and the value at the 95.5th percentile of distances relative to the LiDAR (Jimenez-Berni et al., 2018).

LiDAR data could be affected by occlusion caused by vegetation elements that stop laser beams from penetrating deeper in the canopy (Hosoi and Omasa, 2006; Wang and Fang, 2020). LiDAR could also be affected by voxel size. Choosing the right voxel size, or resolution, is important because the selected resolution plays a role in shape detection, computational efficiency, and object recognition. Going for a voxel size that is too small can lead to redundant data and decreased efficiency, while a larger size may cause distinct objects to be grouped, impacting the performance of algorithms (Ross et al., 2022). Voxel size also affects the gap fraction (Cifuentes et al., 2014), gap fraction indicates the probability of a beam penetrating a canopy and reaching the local normal (Tian and Qu, 2023). LiDAR detects the vertical structure of the canopy directly (Lim et al., 2003; Wang and Fang, 2020) using multiple viewing (Roosjen et al., 2018).

3 Objectives

The objectives of this study were to analyze how changes in the sun's azimuth angle and time of day influenced the computation of LAI values. Another objective focused on developing a non-destructive method for estimating LAI accomplished through the development of linear regression models. These models incorporated metrics extracted from NIR and visible light images, alongside the date as a proxy for the maturity of the wheat canopy.

Furthermore, the precision of LAI estimation was assessed by comparing canopy coverage calculated from NIR images with that from visible light images. The final objective involved determining whether employing distinct models for different wheat varieties could enhance LAI estimation accuracy compared to using a single model for all varieties. To pursue this, wheat varieties were grouped into clusters, and distinct models were established for each cluster.

4 Methods

A 32-variety wheat panel was used in this study, grown at an Agriculture and Agri-Food Canada research farm east of Saskatoon, SK in the season of 2022. These varieties were planted in five randomized replicate blocks, with a seeding date of May 23, 2022. The research field covered an area of approximately 0.076 hectares, with a central location at 52.182415° N latitude and -106.5102015° E longitude. The dataset utilized in this study was gathered from this specific field environment, which comprises five distinct blocks. In each block, there were 32 plots, each specifically assigned to a unique plant variety. It is important to emphasize that although the same 32 varieties were consistently present across all five blocks, their arrangement varied within each block. Essentially, the dataset comprised 32 distinct plant varieties, with each variety replicated five times and distributed across different blocks. The field layout was designed in a serpentine format. Each block of plots alternated between upward and downward patterns as shown in Figure 4.1, with a guard row at both the beginning and end of each block. There is an alley situated between each block and nestled between every plot, bold and thicker black lines, as illustrated in Figure 4.1. All plots were measuring 0.9 m in width and 3.35 m in length.

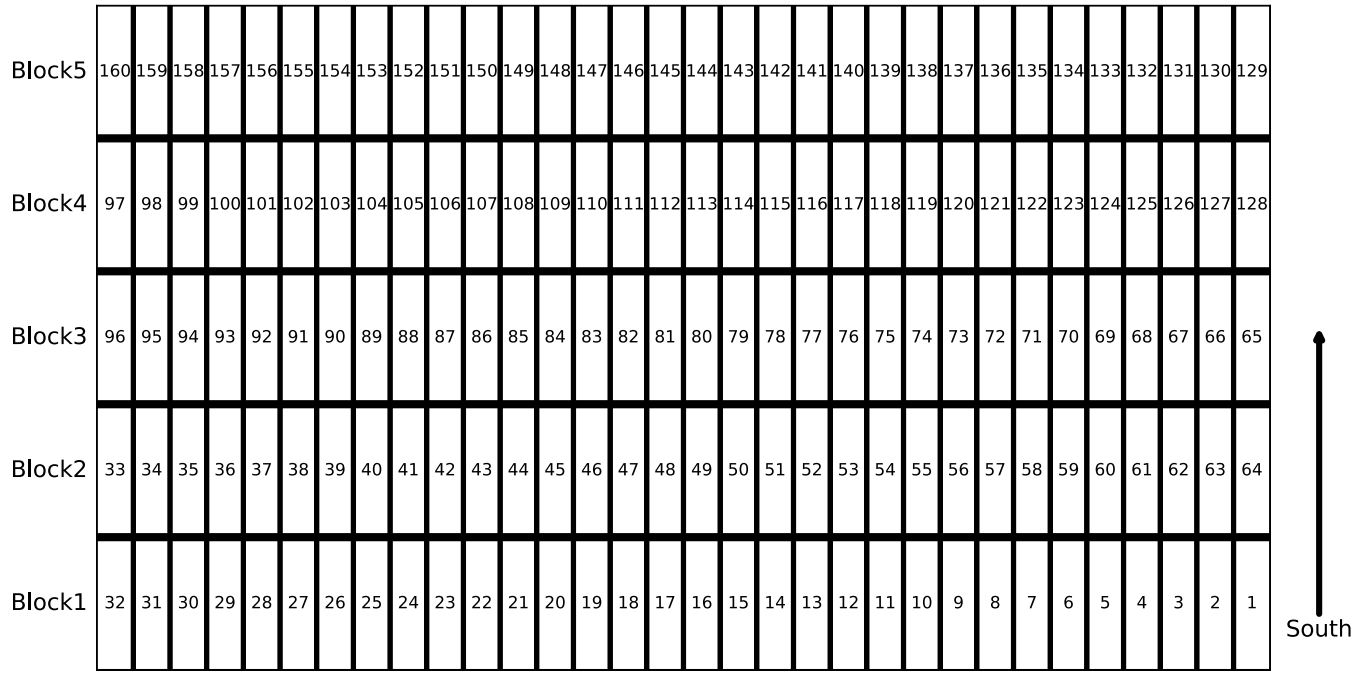

Figure 4.1: Field Plot Layout.

The data collection took place on August 4th, 9th, 12th, 16th, and 25th, 2022. Wheat was in the dough stage on August 4th, 9th, 12th, and 16th, and ripening on August 25th. To nondestructively estimate LAI, RGB and NIR images, LiDAR, and line quantum sensor data were collected. $\mathrm{LAI_{PAR}}$ (LAI values derived from the PAR readings) was calculated using PAR readings from the line quantum sensor, and azimuth angle correction was applied to refine these $\mathrm{LAI_{PAR}}$ values. Height was determined from LiDAR data, and canopy coverage was assessed using image data, specifically NIR and visible light images. Models were then developed, utilizing height and coverage as inputs for the estimation of $\mathrm{LAI_{MODEL}}$.

Figure 4.2: UFPS (USASK Field Phenotyping System)

To collect line quantum sensor data, the LI-COR LI-191R line quantum sensor (LI-COR Inc., Lincoln, NE, USA) and LI-COR LI-250 light meter (LI-COR Inc., Lincoln, NE, USA), as shown in Figure 4.3, were used. Readings from line quantum sensor were compared with those from other PAR sensors that had been previously calibrated. The performance of these sensors was evaluated in both sunny and shaded environments. It was demonstrated that the measurements obtained from the line quantum sensors were largely consistent with those from the calibrated sensors. Consequently, further calibration of the line quantum sensor was not required.

To collect imaging and LiDAR data, the University of Saskatchewan Field Phenotyping System (UFPS), shown in Figure 4.2, was used. Instruments used to complete this study were LIVOX MID70 for LiDAR data and FLIR/Point Grey 5MP Chameleon Cameras for imaging data. FLIR/Point Grey 5MP Chameleon Cameras equipped with 5MP Kowa LM16JC5M2 lenses (Kowa Co., Ltd., Tokyo) and OD 2.0 longpass filters (Edmund Optics Incorporated, Barrington, New Jersey). A color model was used for RGB data, and a monochrome model with a 700 nm OD 2.0 longpass filter was used for NIR images.

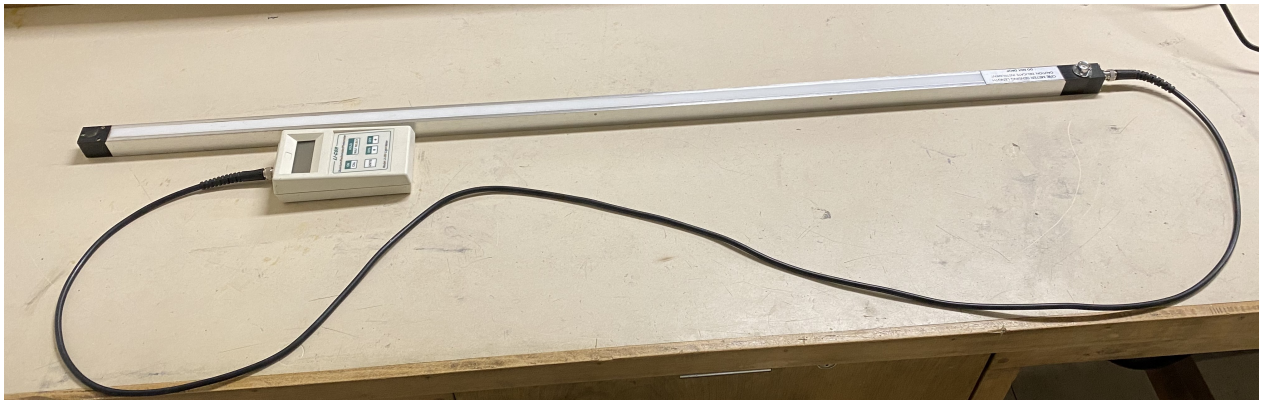

Figure 4.3: LI-COR line quantum sensor and LI-COR LI-250 light meter

4.1 Taking PAR Readings and Calculating LAI_{PAR} Values

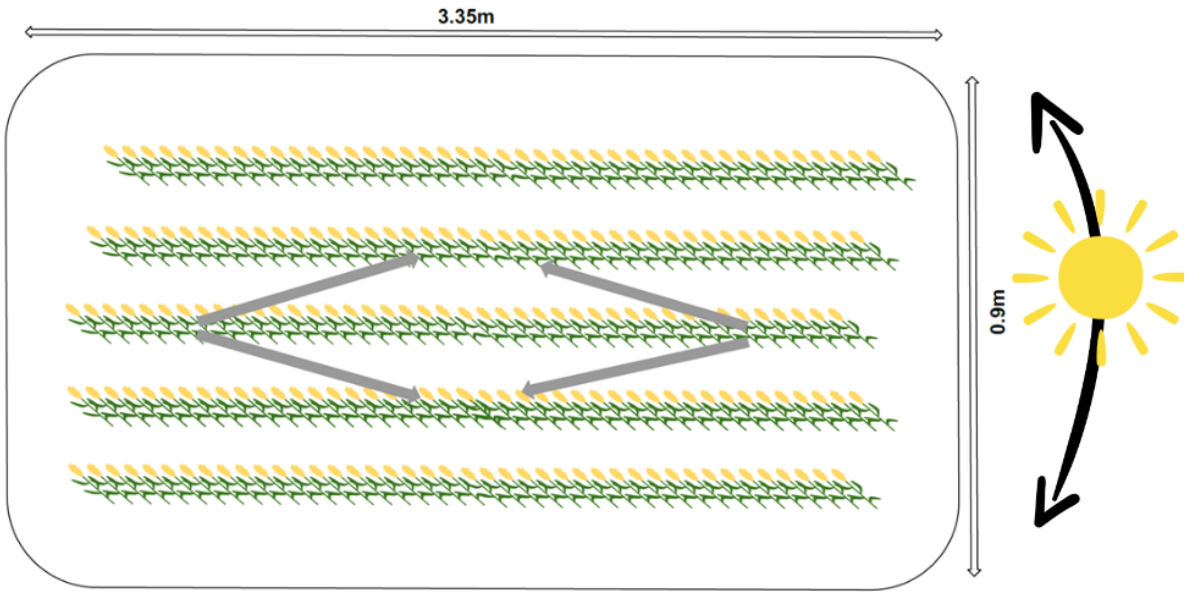

Figure 4.4: Positioning of the line quantum sensor in each plot for below canopy PAR readings.

LAI_{PAR} values for each plot were estimated using PAR readings from the LI-COR line quantum sensor (LI-COR Inc., Lincoln, NE, USA) connected to the LI-COR LI-250 light meter (LI-COR Inc., Lincoln, NE, USA) on 4, 9, 12, 16, and 25 August 2022, spanning from around 9:30 AM to 2:30 PM on each day, during predominantly sunny weather conditions. The field had 5 blocks and PAR readings were taken from Block 1 and Block 2. In each plot in the first two blocks, four below-canopy PAR readings were taken after one above-canopy reading (Facchi et al., 2010; Wilhelm et al., 2000). For each below-canopy PAR reading, the line quantum sensor was positioned as suggested in the AccuPAR LP-80 manual, starting on one row and ending on the next row. As shown in Figure 4.4, middle rows were selected for below-canopy PAR readings (Facchi et al., 2010; Wilhelm et al., 2000) to reduce edge effects, which is the difference in growth between plants located on the external borders and plants located in the internal regions (Wang et al., 2013). The four below-canopy PAR readings were averaged to obtain the below-canopy PAR value (Decagon, 2013) and LAI_{PAR} values were determined following the methodology outlined in Section 2.1.

4.2 Azimuth Angle Correction

The time of data collection and the sun azimuth angle may lead to bias in the calculation of the LAI (Salter et al., 2018). The correction of LAI_{PAR} values was achieved through a mathematical operation as Equation 4.1, conducted separately for each data collection date instead of applying all the data together. This process involved subtracting the predicted LAI values (LAI_{GAM}), derived from a Generalized Additive Model (GAM), from the LAI_{PAR} values. Subsequently, the population mean of the LAI_{PAR} values ($\overline{LAI}_{PAR}$) were added to the obtained result. The GAM was employed as a regression-based methodology, adept at capturing and accommodating the nonlinear trends between the sun azimuth angle and LAI_{PAR} values (Pinilla and Negrín, 2021). The pyGAM library is used to implement the GAM model (pyGAM documentation, nd). In the GAM model, the way each feature interacts with the target is shaped by the 'terms' parameter. It was set to 'auto', which automatically assigns a univariate spline term to each feature. This approach captures nonlinear patterns without the need for explicit instructions. Additionally, the default 'max_iter' parameter was employed, defining the maximum number of iterations for the optimization algorithm during model fitting, which is set to 100 iterations.

Figure 4.5 and the correction process showcase an example dataset created for illustrative purposes, providing a demonstration of the correction steps applied to LAI_{PAR} values with respect to Sun Azimuth Angle. Figure (a) represents the initial state, presenting a scatter plot of the raw data, which corresponds to the measured LAI_{PAR} values, emphasizing the raw relationship between LAI_{PAR} and azimuth angles. Figure (b) introduces the GAM fit, revealing patterns within the artificially generated data. Figure (c) then portrays the LAI_{AZ} values resulting from a correction process. The correction involves subtracting the predicted LAI values derived from the GAM model from the LAI_{PAR} values. Subsequently, the population mean of the LAI_{PAR} values are added to the result.

$$LAI_{\mathrm{AZ}} = LAI_{\mathrm{PAR}} - LAI_{\mathrm{GAM}} + \overline{LAI}_{\mathrm{PAR}} \tag{4.1}$$

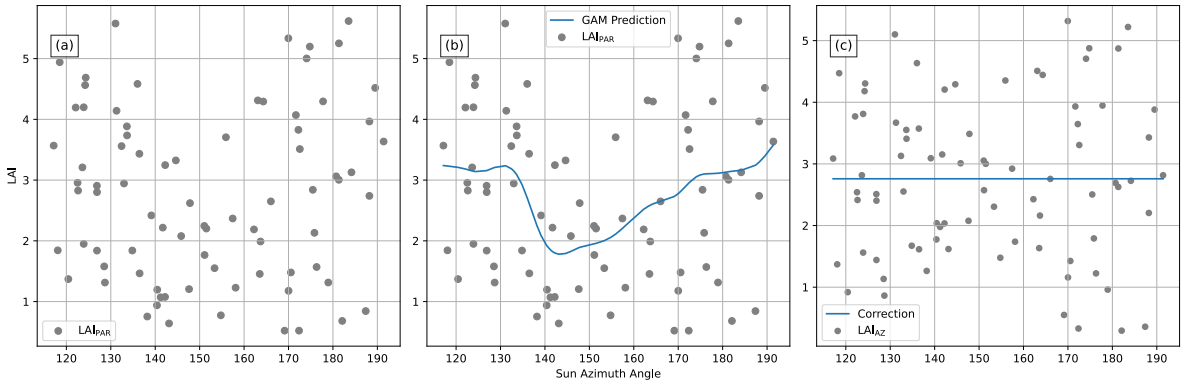

Figure 4.5: The correction process for $\mathrm{LAI}_{\mathrm{PAR}}$ values based on Sun Azimuth Angle. (a) Original data displays the raw relationship between $\mathrm{LAI}_{\mathrm{PAR}}$ and azimuth angles. (b) The GAM fit captures patterns in the data. (c) Corrected data emerges by subtracting the predicted LAI values, derived from the GAM, from the $\mathrm{LAI}_{\mathrm{PAR}}$ values, followed by the addition of the population mean of the $\mathrm{LAI}_{\mathrm{PAR}}$ values.

4.3 Height Calculations

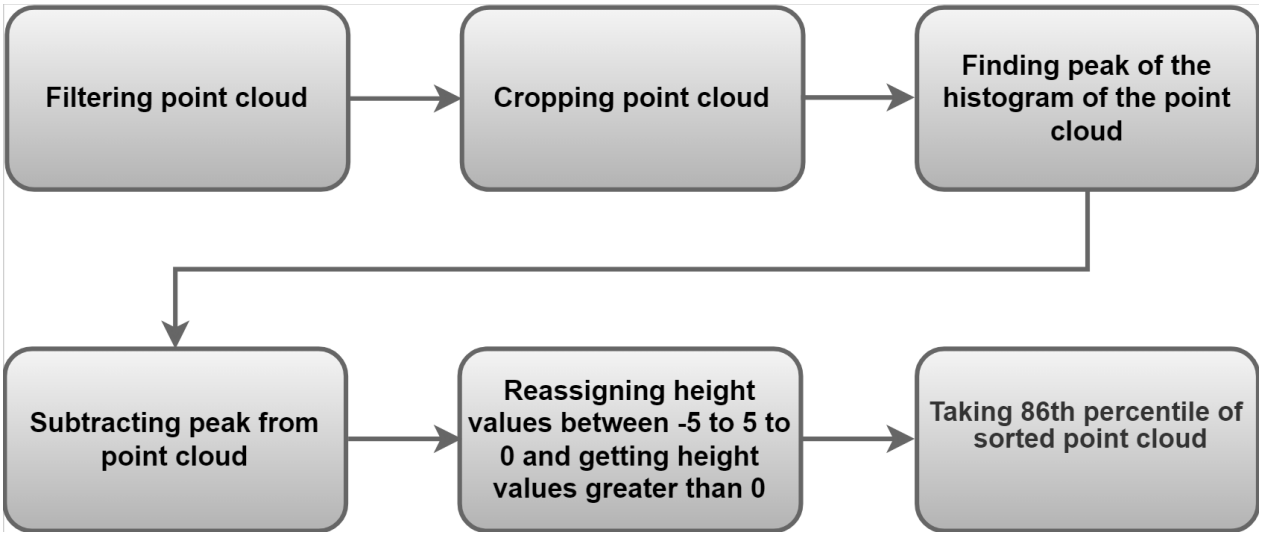

Figure 4.6: The flowchart of deriving the height of a wheat plant utilizing LiDAR data.

The process of deriving the height of a wheat plant utilizing LiDAR data involved several steps, as shown in Figure 4.6. The point cloud data from each plot, captured by the LiDAR sensor, was filtered to remove statistical outliers. This step removed points in the point cloud that were farther than the average distance from neighboring points using Open3D library (Open3DKey, nd). A neighborhood of 32 points was used. Subsequently, a threshold level equivalent to 2 standard deviations was applied to the average distances across the entire point cloud. This ensured that points further away from their neighbors than the computed threshold were considered outliers and consequently removed from the point cloud. The height of the point cloud data was used to create the histogram, and this was where the histogram's peak was located. As more ground data was available, this peak was designated as ground level (Jimenez-Berni et al., 2018; Madec et al., 2017). While the peak of the histogram is frequently referred to as the ground level, it should be noted that there is no guarantee that the ground will have the most points in the histogram. The value in the histogram that has the most points might not always represent the ground due to changes in the terrain, the presence of elevated structures, or other anomalies in the data. Accurate ground-level identification was ensured in the dataset under study, as the highest return consistently aligned with the ground level. Subsequently, the data were cropped to a 0.5 x 1m area to remove edge effects. Cropping was done after creating a histogram, prioritizing the accurate determination of ground level. Subtracting the peak value of the histogram from the point cloud data gave us the actual canopy height because the LiDAR sensor combined with GPS gives the point cloud height values relative to sea level. Returns from raised soil along seeding furrows, rocks, or other miscellaneous objects, and small holes were eliminated. An estimation of the total canopy height can be obtained from the 86th percentile of the preprocessed and sorted point cloud (Walter et al., 2019).

4.4 Canopy Coverage Calculations

The amount of plant leaves that cover the soil's surface, also known as the canopy cover, is frequently measured in research on photosynthesis, transpiration, and erosion (Armbrust, 1990). The general canopy coverage formula used for image data was:

$$Canopy\ Coverage(\%) = (Vegetation\ pixels)/(Total\ pixels) * 100 \tag{4.2}$$

In this research, NIR light images and visible light images were used to identify pixels containing vegetation.

4.4.1 Canopy Coverage Calculations Using NIR Images

In healthy plants, a high percentage of light in the near-infrared region is reflected from leaves (Knipling, 1970). The process of deriving the canopy coverage of a wheat plant utilizing NIR images involved creating a binary image using thresholding. In this study, Otsu's method, an automatic image thresholding technique,

was utilized to derive a single-intensity threshold. The threshold utilized aims to minimize intraclass variance between thresholded black and white pixels while maximizing the separation between foreground (vegetation) and background (soil) pixels (Otsu, 1979). In Figure 4.7, the left image is the NIR image of the plot, and the right image is the binary image generated using thresholding, where black pixels represent vegetation, and white pixels represent the background. The range of canopy coverage varied between 11.46% and 57.20%.

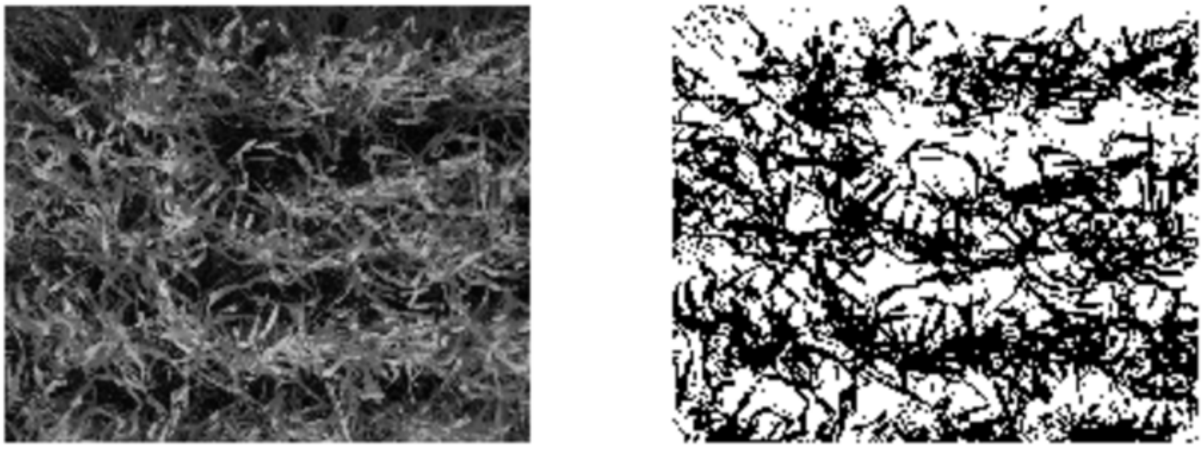

Figure 4.7: Creating a binary image from an NIR image using thresholding.

4.4.2 Canopy Coverage Calculations Using Visible Light Images

Pixels of vegetation were found using RGB images that had been converted to CIELAB color space images. The L* axis stands for lightness. The b* axis has a range from blue (-b) to yellow (+b), while the a* axis has a range from green (-a) to red (+a) (Guiné et al., 2015). Unsupervised machine learning techniques like K-means clustering aim to split a given dataset into K groups, where K is specified. Each data point is assigned to the cluster with the closest center, according to the similarity metric. This process is iterated on, updating the cluster centers each time until they converge (Ikotun et al., 2023). In this study, channel b was utilized to cluster senescent vegetation as it represents the yellow color, while channel a was used to cluster green vegetation due to its representation of green color. Initially, the pixels of the plot image were categorized as either senescent vegetation or background based on the analysis of channel b in the image. Following this, another round of classification occurred, this time designating pixels as either green vegetation or background, relying on the channel a of the image. Any remaining pixels that did not fall into the senescent or green vegetation categories were classified as background pixels. Figure 4.8 shows how k-means clustering was used to divide the image into two categories: senescent vegetation and green vegetation. The remainder of the pixels were labeled as background. The left image represents the original image. The right image displays green vegetation highlighted in green, senescent vegetation in yellow and the background in black.

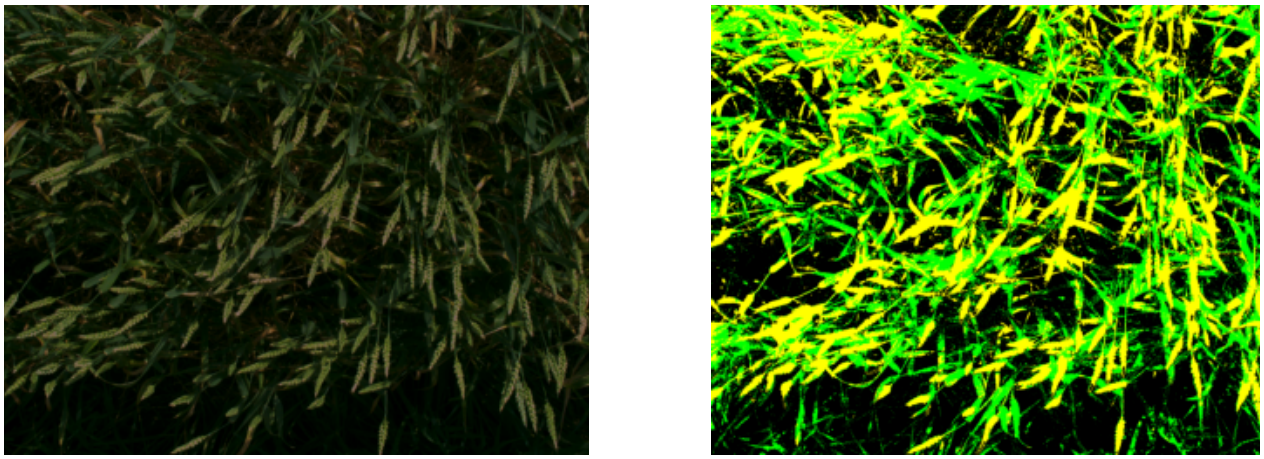

Figure 4.8: Creating a segmented image from CIELAB image using a k-means clustering algorithm.

4.5 Model Creation

To investigate the relationship between one or more independent variables and a continuous outcome, linear regression models are frequently employed (Schmidt and Finan, 2018). Linear regression modeling is a reliable data analysis method that can be utilized for several different tasks such as prediction and data interpretation (Hoff, 2009). A linear regression analysis was used in this study to determine the relationship between height, canopy coverage, maturity proxy, and LAI using data from the first two blocks of the field. The model creation process used the Scikit-learn library (Scikit-Learn, nd) in Python involved splitting the data into training and test sets. When splitting the dataset, the 'random_state' parameter was set to a fixed value, ensuring consistent random splitting each time the code was executed. Additionally, a 'test_size' parameter of 0.3 indicated that 30% of the data was allocated for testing, leaving 70% for training the model. Even though there were five blocks in total, the data were from Block 1 and Block 2, as only the PAR readings from these blocks were accessible. Subsequently, the model was constructed by fitting the training data. The evaluation phase utilized test data to calculate performance metrics, including root mean squared error (RMSE) and adjusted coefficient of determination (R^2). RMSE is a measure of the average absolute disparity between predicted and actual values. A model is considered improved with a decrease in the RMSE value. An RMSE of zero indicates a perfect model that predicts the exact target value (Chicco et al., 2021). The R^2, also often referred to as goodness of fit, measures how a given set of input variables explains the variation in output and can overestimate how well the linear regression fits. It remains unchanged or rises as more variables are incorporated into the model. To account for this overestimation, adjusted R^2 is used. It is possible for the adjusted R^2 value to decrease if that variable does not improve the model (Schroeder et al., 1986; Bar-Gera, 2017). The Adjusted R^2 value is less than R^2, and an adjusted R^2 value 1 implies that the model correctly predicts values of the target field, whereas a value of 0 or less implies a model that is not capable of making

predictions (Chicco et al., 2021). In the final step, a comparison of models was conducted based on these evaluation metrics, providing insights into their predictive accuracy and overall performance. (For the model parameters and evaluation metrics of the developed models, refer to Table A.1.)

5 Results and Discussion

In this chapter, within the section on 5.1, the effect of changes in the azimuth angle of the sun on LAI_{PAR} values was discussed. In section 5.2, an examination is made regarding the impact of utilizing LAI_{PAR} and LAI_{AZ} values as outputs in the model. Additionally, consideration was given to the impact of incorporating visible light image-based canopy coverage and NIR image-based canopy coverage as input parameters. Furthermore, attention was directed towards the impact of including height and date as input parameters in the model. In the section on the 5.3, the significance of wheat varieties in determining LAI was highlighted, and various models were compared.

5.1 PAR Readings, LAI, and Azimuth Angle

The Generalized Additive Model (GAM) algorithm (pyGAM documentation, nd) was used to test the hypothesis that LAI_{PAR} values are significantly impacted by the changes in the azimuth angle of the sun and, therefore the time of day. Models were constructed using LAI_{PAR} data and LAI_{AZ} determined from LAI_{PAR} and the corresponding sun azimuth angle. The p-value of the azimuth angle term was provided by the model. The same approach was used to assess the significance of the sun azimuth angle on the LAI_{AZ}, according to the method outlined in the section 4.2.

Table 5.1: Statistical significance of Sun Azimuth Angle's impact on LAI_{PAR} and LAI_{AZ}. * denotes significance when the p-value is less than or equal to 0.05.

GAM Input	**GAM Output**	**P-Value**
Sun Azimuth Angle	LAI_{PAR}	1.11e-16*
Sun Azimuth Angle	LAI_{AZ}	0.246

A p-value less than or equal to 0.05 was chosen as the significance level. The analysis showed that the azimuth angle had a statistically significant impact on LAI_{PAR} as shown in Table 5.1. This suggests that the azimuth angle of the sun was a key factor in determining the variation in LAI_{PAR} values. According to further analysis, there was no statistically significant relationship between azimuth angle and LAI_{AZ} as shown by p-value in Table 5.1. Therefore, it was concluded that the correction procedure eliminated the sun azimuth angle effect.

In this analysis, it is important to note that the dataset was constrained to a single year and may not

capture the full spectrum of growth stages in the canopy. The data were limited to a brief range, making it challenging to comprehend the development of the canopy over the season. Additionally, the azimuth correction analysis technique employed was data-driven, implying that the findings are reliant on the available data and may not encompass complexities, such as variations across different growth stages or different years, which were not provided by the given dataset.

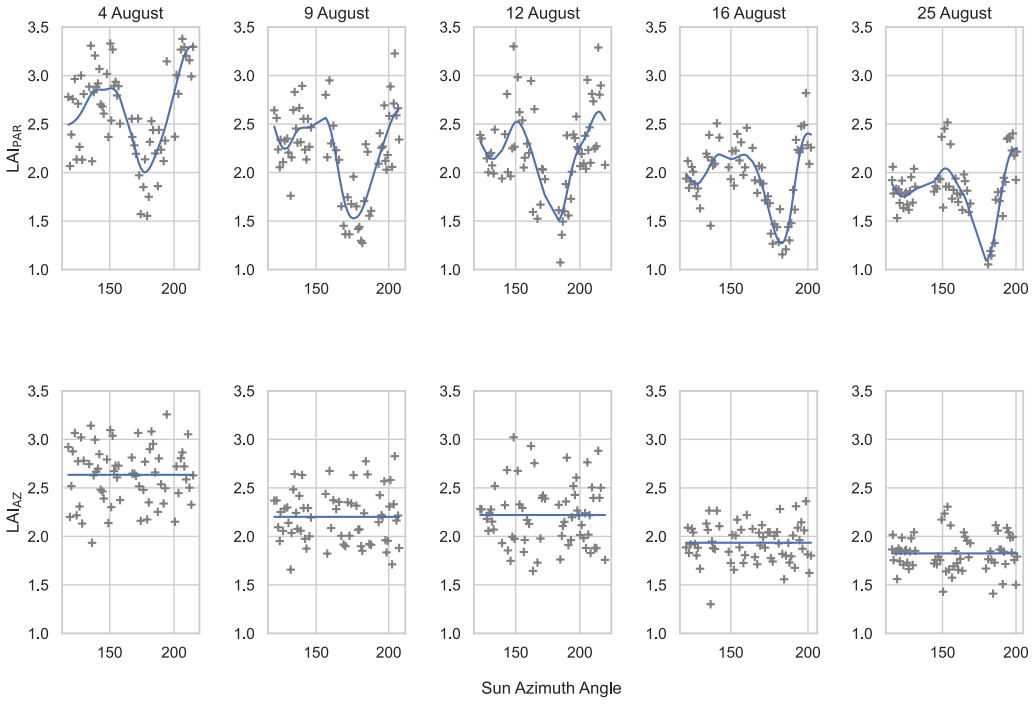

Figure 5.1: Visualization of the relationship between LAI values and sun azimuth angle for each day data was collected, with the line indicating the model fit. Top row: $\mathrm{LAI_{PAR}}$ values (no azimuth correction). Bottom row: Corrected $\mathrm{LAI_{AZ}}$ values.

Figure 5.1 shows the relationship between the $\mathrm{LAI_{PAR}}$ and sun azimuth angle following the data collection and calculation of $\mathrm{LAI_{AZ}}$ values. The azimuth angle of the sun is represented on the x-axis in both rows. The first row plots the calculated $\mathrm{LAI_{PAR}}$ values versus azimuth angle in the way previously discussed in section 4.1, while the second row's y-axis shows the $\mathrm{LAI_{AZ}}$ values as explained in the section 4.2. According to the top row of the provided Figure 5.1, the findings revealed a pattern in the relationship between $\mathrm{LAI_{PAR}}$ and sun azimuth angle throughout individual dates as well as when data were analyzed collectively. The correction applied reveals that no discernible sun azimuth effect exists within the second row of Figure 5.1

that demonstrates consistent results in the same direction through statistical analysis.

Figure 5.2 compares LAI data that have not been corrected for sun azimuth angle (LAI_{PAR}) and corrected for sun azimuth angle (LAI_{AZ}) for 32 varieties on the date August 16th. Each variety has two corresponding LAI_{PAR} and LAI_{AZ} values because PAR readings were taken from two blocks of each variety.

From a visual analysis of Figure 5.2, it became evident that the corrected values in Figure 5.2 are more consistent in most cases. The adjustments made to the LAI_{AZ} values in Figure 5.2 allowed for a better understanding of the characteristics of varieties. In contrast to the LAI_{PAR} values, LAI_{AZ} values of the varieties within a given date exhibit closer proximity to each other. This showed that the variation among the varieties has been decreased by the LAI_{AZ} values in Figure 5.2. The LAI_{PAR} values taken from first two blocks exhibit a standard deviation of 0.51, encompassing all the collection dates. Meanwhile, the LAI_{AZ} values taken from the first two blocks demonstrate a standard deviation of 0.38 across the entire set of data collection dates. LAI_{AZ} values are more consistent and closely clustered, outlining a more consistent behavior among the varieties than LAI_{PAR} values.

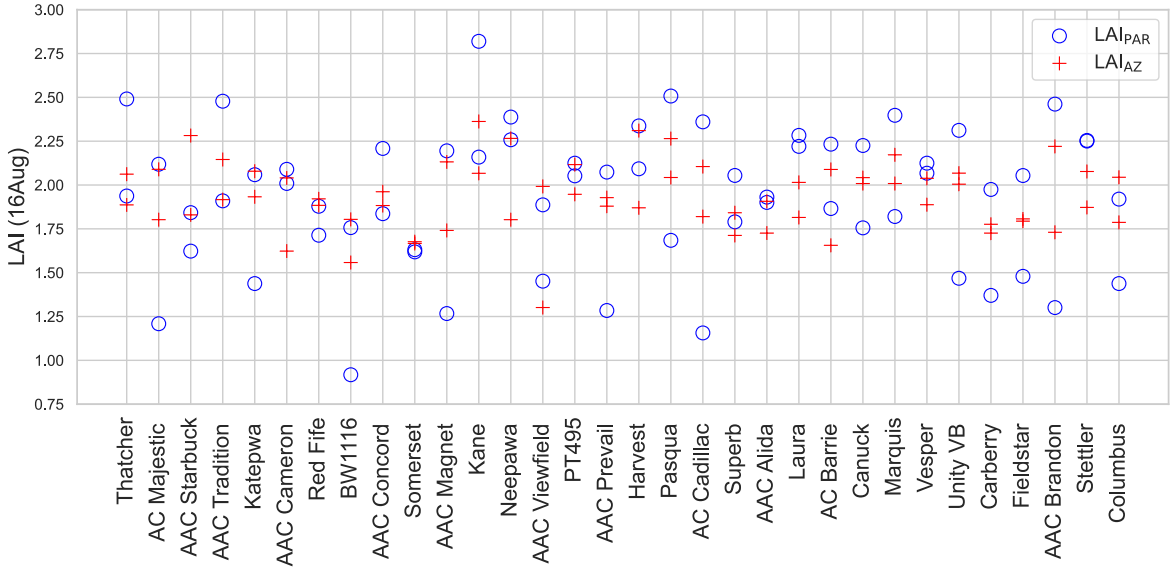

Figure 5.2: Relationship between LAI_{PAR} and LAI_{AZ} values across varieties on August 16. For plots of remaining dates, refer to Appendix A.

The period between August 4th and August 25th marked the maturation phase of the crop, resulting in a decrease in LAI_{PAR} and LAI_{AZ} values. Table 5.2 shows the mean value of the LAI_{PAR} and LAI_{AZ} values, which were calculated for a specific date, and also shows a decline in these values over time (Salter et al., 2018).

Table 5.2 illustrates the mean of LAI_{PAR} values and LAI_{AZ} values for each date in the 'Mean' column. The mean of LAI_{PAR} and LAI_{AZ} values are the same because the correction process preserved the overall

distribution. Because only two data points of LAI_{PAR} for each variety on each date were available, the absolute difference between these values was calculated, and the mean of these values for each date and the mean of these values overall were calculated. The overall mean intra-variety differences in LAI_{PAR} values, was 0.46, while the overall mean intra-variety of differences of LAI_{AZ} values was 0.24. These means indicate that after the correction, the data points for each variety on specific dates had become closer. The mean of the absolute difference between two data points of LAI_{PAR} and LAI_{AZ} values for each variety on each date was calculated and shown in the 'Mean Intra-variety Diff.' column while the standard deviation of these values is shown in the 'Standard Deviation of Intra-variety Diff.' column. These data align with the behavior of the overall mean values, indicating that the differences are progressively decreasing as the dates progress.

Table 5.2: Mean LAI and standard deviation values of the LAI_{PAR} and LAI_{AZ} calculated for specific dates.

Date	**Mean**	$LAI_{\mathbf{PAR}}$		$LAI_{\mathbf{AZ}}$	
		Mean Intra-variety Diff.	**Standard Deviation of Intra-variety Diff.**	**Mean Intra-variety Diff.**	**Standard Deviation of Intra-variety Diff.**
04-Aug	2.63	0.54	0.35	0.28	0.25
09-Aug	2.20	0.52	0.42	0.28	0.22
12-Aug	2.22	0.39	0.31	0.24	0.18
16-Aug	1.93	0.47	0.34	0.23	0.17
25-Aug	1.82	0.36	0.30	0.20	0.15
Overall	2.16	0.46	0.35	0.24	0.20

The relationship between time and the azimuth angle of the sun is significant, yet it is not a simple, uniform correlation. Calculating the sun's azimuth angle involves considering various factors such as the year, day, hour, longitude, and latitude (Michalsky, 1988). Analyzing the time of day effect on LAI enables the identification of temporal shifts and daily patterns while examining sun azimuth angle allows for the detection of temporal changes and daily trends of LAI measurements due to the sunlight's direction.

LAI_{PAR} calculation may be influenced by the timing of data collection (Salter et al., 2018). The significance of time of the day was evaluated for both the LAI_{PAR} and LAI_{AZ} using a method that was similar to the one used to determine sun azimuth angle significance. This shows that time of day had a significant impact on LAI_{PAR} but not on LAI_{AZ} as shown in Figure 5.3. Thus, suggests that the influence of the time of day was removed by the sun azimuth angle correction.

The plots were arranged in a north-south direction in the field. Between 12:00 and 13:00, the influence of time of day becomes more noticeable as shown in Figure 5.3. This effect is also noticeable between 13:00 and 14:30. However, before 12:00, the impact of time of day is more subtle. Considering these observations,

it is advisable to take measurements before 12:00 when the influence of time of day is less noticeable. It is important to note that this suggestion specifically applies to plots aligned from north to south. The situation may differ for plots oriented from east to west, and similarly, variations may arise based on the latitude and longitude of the plots.

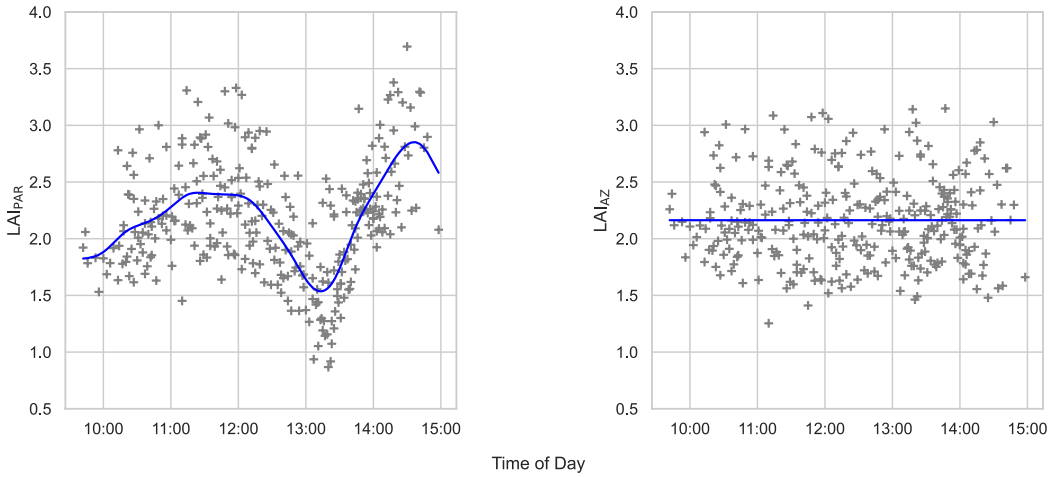

Figure 5.3: Left plot: Relationship between $\mathrm{LAI_{PAR}}$ values and time of day. Right plot: Relationship between $\mathrm{LAI_{AZ}}$ values and time of day.

5.2 Estimating LAI from Canopy Coverage with Single Model

To estimate LAI from canopy coverage, linear regression models were utilized. The impact of various input and output parameters was assessed using evaluation metrics. For model parameters and evaluation metrics of the developed models, refer to Table A.1.

5.2.1 Prediction of $\mathrm{LAI_{PAR}}$ versus $\mathrm{LAI_{AZ}}$

Preliminary models were created to evaluate the impact of using various LAI values. In these models, the outputs were $\mathrm{LAI_{PAR}}$ and the $\mathrm{LAI_{AZ}}$ while the input was canopy coverage obtained from NIR images. As shown in the Table 5.3 the RMSE for the $\mathrm{LAI_{PAR}}$ and $\mathrm{LAI_{AZ}}$ models were 0.41 and 0.29, respectively. These results suggest that the RMSE metric favored the model using $\mathrm{LAI_{AZ}}$. Models were also assessed using the adjusted R^2. The adjusted R^2 for the $\mathrm{LAI_{PAR}}$ model was 0.39, however, the adjusted R^2 for the $\mathrm{LAI_{AZ}}$ model was 0.5. These results suggest that the adjusted R^2 metric, like the RMSE, also favored the $\mathrm{LAI_{AZ}}$ model. These results led to the selection of $\mathrm{LAI_{AZ}}$ for future use.

Table 5.3: Model results comparing the impact of using various LAI values as an output parameter with canopy coverage as an input parameter.

Model Input	**Model Output**	**Adjusted R^2**	**RMSE**
Canopy Coverage	LAI_{PAR}	0.39	0.41
Canopy Coverage	LAI_{AZ}	0.50	0.29

5.2.2 The Impact of Visible versus NIR-Image Based Canopy Coverage

Correlations in Table 5.4 indicate a stronger correlation between LAI_{AZ} and NIR image-based canopy coverage compared to colour image-based green canopy coverage or colour image canopy coverage containing green and senescent vegetation. It was hypothesized that canopy coverage calculated from NIR images may yield a more accurate calculation of LAI compared to canopy coverage calculated using visible light images. In comparison to visible light, near-infrared radiation can travel farther through the canopy due to its low absorptance and high transmittance. Therefore, the amount of near-infrared radiation reflected into the atmosphere will depend on how much overlap there is between leaves in a canopy. This is because as the canopy gets denser, much of the near-infrared radiation will become progressively scattered (Jensen, 1980). To test this hypothesis, three models were developed using NIR image-based canopy coverage, colour image-based green canopy coverage, and colour image canopy coverage containing green and senescent vegetation. The RMSE value of the NIR-based model was 0.29 for the NIR canopy coverage input. The colour image-based coverage models resulted in RMSE values of 0.41 and 0.40 for colour image based green coverage and canopy coverage containing green and senescent vegetation, respectively. The adjusted R^2 value of the NIR-based model was 0.50. Colour image based coverage models resulted in adjusted R^2 values of -0.04 and 0.01 for colour image based green coverage and canopy coverage containing green and senescent vegetation, respectively. Small R^2 values will result in a negative adjusted R^2 value (Leach and Henson, 2007), which means that the model's ability to predict is poor. These results led to the selection of the canopy coverage obtained from NIR images (referred to as canopy coverage for the remaining of the project). Reasons for the disparity between NIR and visible image performance may include the approach taken in developing the segmentation algorithm.

5.2.3 The Impact of Height on LAI Prediction

Height is a common parameter in LAI models (Zhang et al., 2019; Yuan et al., 2013). Height was therefore tested as an input to a LAI_{AZ} model, both alone and in combination with canopy coverage metrics. Each model used LAI_{AZ} as its output parameter. The model with a single input of canopy coverage had an adjusted R^2 value of 0.50 and RMSE of 0.29. The model that only took height as an input, on the other hand, had an adjusted R^2 value of -0.08 and an RMSE value of 0.42. The model using inputs for both height and canopy coverage had an adjusted R^2 value of 0.47 and an RMSE value of 0.29. This indicates that using height alone

was not as reliable as using only canopy coverage for prediction. Additionally, including height alongside canopy coverage in the model did not lead to any improvement in this study. When the plant height was nearly at its maximum, the LAI reached its highest. In this study, field measurements were made when the wheat was in its late stages of development, specifically in the dough and ripening stages. The fact that the height has already reached its maximum value could be the reason why adding height as an input did not improve the model's ability to forecast. Correlations in Table 5.4 are consistent with the model's evaluation metrics. For further analysis, the model that only used canopy coverage as an input was preferred over the model that also used height as an input despite having similar RMSE values because of its higher adjusted R^2 value.

Table 5.4: Correlation coefficients between Height, Canopy Coverage metrics and LAI_{AZ}. CC denotes canopy coverage.

	Height	**NIR CC**	**L*a*b* Vegetation CC**	**L*a*b* Vegetation and Senescent CC**	**LAI_{AZ}**
Height	1.00	-0.04	-0.03	-0.03	0.04
NIR CC	-0.04	1.00	-0.10	-0.25	0.64
L*a*b* Vegetation CC	-0.03	-0.10	1.00	0.42	-0.11
L*a*b* Vegetation & Senescent CC	-0.03	-0.25	0.42	1.00	-0.18
LAI_{AZ}	0.04	0.64	-0.11	-0.18	1.00

5.2.4 The Impact of Date

The main goal of this section of the research was to establish the significance of the date of data collection on LAI estimation. This was accomplished with a GAM using the date as the input and LAI_{AZ} as the output to capture the nonlinear trends between date and LAI_{AZ}. Several statistical indicators, including p-values, were acquired throughout the model-fitting procedure (Salter et al., 2018). The p-value for the date variable, standing at 1.11e-16, showed that it was statistically significant.

The data were separated into distinct subsets for each date based on the analysis results. The canopy coverage was used as an input, and LAI_{AZ} was used as an output to generate a unique model for each individual day. For each date, the RMSE and adjusted R^2 values are shown in Table 5.5. These results show that there was a poor fit in the models. Considering this, the decision was made not to employ distinct models for each date, as it was found that the predictive power of the model was limited within date variability. This could be due to insufficient data to create five distinct models that exhibit a good fit. Another potential factor influencing the results could be the relatively narrow timeframe between the dates of data collection.

Table 5.5: Model results comparing LAI prediction when data were separated into distinct subsets for each date.

Date	**Adjusted R^2**	**RMSE**
04-Aug	-0.64	0.28
09-Aug	0.03	0.23
12-Aug	-0.21	0.28
16-Aug	-0.06	0.19
25-Aug	0.12	0.18

Given that the date was statistically significant for LAI, a model was developed that included both NIR canopy coverage and date as a proxy for maturity. The first date (August 4) of data collection was designated as day 1, with subsequent days incrementing sequentially. Models were developed utilizing either just canopy coverage alone or a combination of canopy coverage and date. As an output parameter, LAI_{AZ} was utilized by each model. It had been determined to retain the model incorporating both date and canopy coverage, as Table 5.6 reveals superior results in terms of RMSE and adjusted R^2 compared to the model solely based on canopy coverage. This outcome might be caused by the inclusion of date as an input variable, which added more information and raised the predictability of LAI. The model can capture the patterns in LAI by using the date as an input, leading to a better fit and more accurate and precise predictions.

After employing the date as a proxy for maturity, the implementation of growing degree day (GDD) aimed to evaluate whether it could enhance the predictive power of the model when utilized as a maturity proxy. GDD represents the daily mean temperature surpassing a base temperature that is conducive to plant growth (Shaykewich, 1995; Saiyed et al., 2009). In the calculation of GDD, the first step is to subtract the base temperature, typically set at 5°C for estimating crop growth in Western Canada, from the average daily temperature. This average daily temperature is determined as the mean between the maximum and minimum air temperatures for a given day. Subsequently, any result falling below zero is treated as zero, ensuring that negative values do not impact the overall cumulative total (Walker, 1989). Table 5.6 illustrates that the utilization of GDD did not yield improvements in the obtained results. The absence of enhancements when utilizing GDD instead of the date implies that the model can capture patterns in LAI using both the date and GDD. The correlation of 0.998 between GDD and date further underscores this insight, highlighting the consistency of the results. However, the lack of noticeable improvements in predictive accuracy when utilizing GDD in place of the date could be due to the restricted data range, which only covers the end of the growing season. Having a dataset that spans the entire growth cycle would allow for a more thorough understanding of the interaction between temperature fluctuations and growth phases.

Table 5.6: Model results comparing LAI prediction using input parameters: Canopy Coverage alone, Canopy Coverage & Date, and Canopy Coverage & GDD.

Model Input	Adjusted R^2	RMSE
Canopy Coverage	0.50	0.29
Canopy Coverage & Date	0.58	0.26
Canopy Coverage & GDD	0.58	0.26

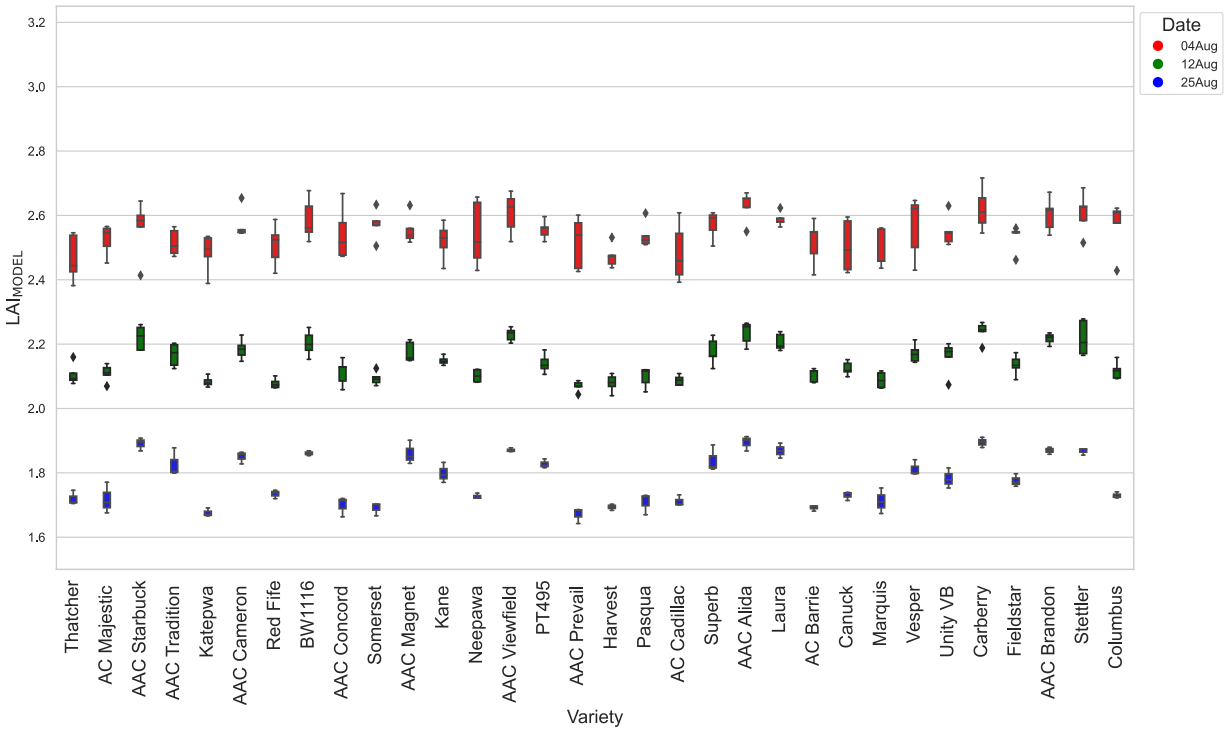

Figure 5.4: Relationship between the $\text{LAI}_{\text{MODEL}}$ values and varieties, where the model incorporates date and canopy coverage as input parameters. For plots of each date, refer to Appendix A Figure A.3.

Models were trained on the two replicate blocks for which LAI measurements were taken with the ceptometer. Due to these limitations in available data, independent testing was limited to evaluating the consistency of estimates and overall trends when models were applied to estimating the LAI of the blocks that did not have ceptometer measurements. Even though models were trained on two blocks, models were used to estimate LAI values for all five blocks by utilizing information extracted from the images of five blocks because

all five blocks were utilized for image collection. For generating the plots in Figure 5.4, the model, trained on the two replicate blocks, utilized information from five blocks of the field to estimate LAI. Each variety in Figure 5.4 was associated with five corresponding predicted $\text{LAI}_{\text{MODEL}}$ values for each data collection date. For the enhancement of clarity and ease of interpretation, three specific dates from the dataset were selected for display. Therefore, Figure 5.4 displays the $\text{LAI}_{\text{MODEL}}$ values for each variety, reflecting the model's estimations based on the date and canopy coverage data from the five blocks of the field. Figure 5.4 shows that the LAI estimation within varieties is relatively consistent.

5.3 Multi-Model Hypothesis Testing

The main goal of this section of the research was to establish whether wheat variety was a significant factor in predicting LAI. The significance of the impact was assessed through the use of a p-value. With a p-value of 0.0461, which is below the threshold of 0.05, the results indicated that LAI was significantly impacted by the variety of wheat. The predictive power of the model could be enhanced by recognizing the impact of variety, which may have been previously overlooked.

After analyzing the significance of variety in predicting LAI, it was decided to remove three specific varieties which considerably reduced the model's ability to fit the data. Three varieties were removed because if too few varieties were removed, it may not enhance the model's performance, while if too many were removed, there could be a risk of information loss or undermining the diversity of the dataset. Datasets were created by removing every combination of three varieties. Models were created using the inputs of date and canopy coverage for each dataset. Based on having the lowest RMSE value and the greatest adjusted R^2 value in comparison to the other models, the best model among the created models was chosen. The best model among the created models was chosen with an R^2 value of 0.63 and an RMSE value of 0.23. This new model, which contained 29 varieties by removing three varieties which were AAC Magnet, AAC Prevail, and Carberry, outperformed the previously selected model, which had an adjusted R^2 value of 0.58 and an RMSE value of 0.26, in terms of performance. Figure 5.5 illustrates the $\text{LAI}_{\text{MODEL}}$ values for each variety. The predictions were based on the date and canopy coverage data from the five blocks of the field. Figure 5.5 displays consistent results with Figure 5.4, as the pattern remains more or less the same and the variability continues to be relatively small.

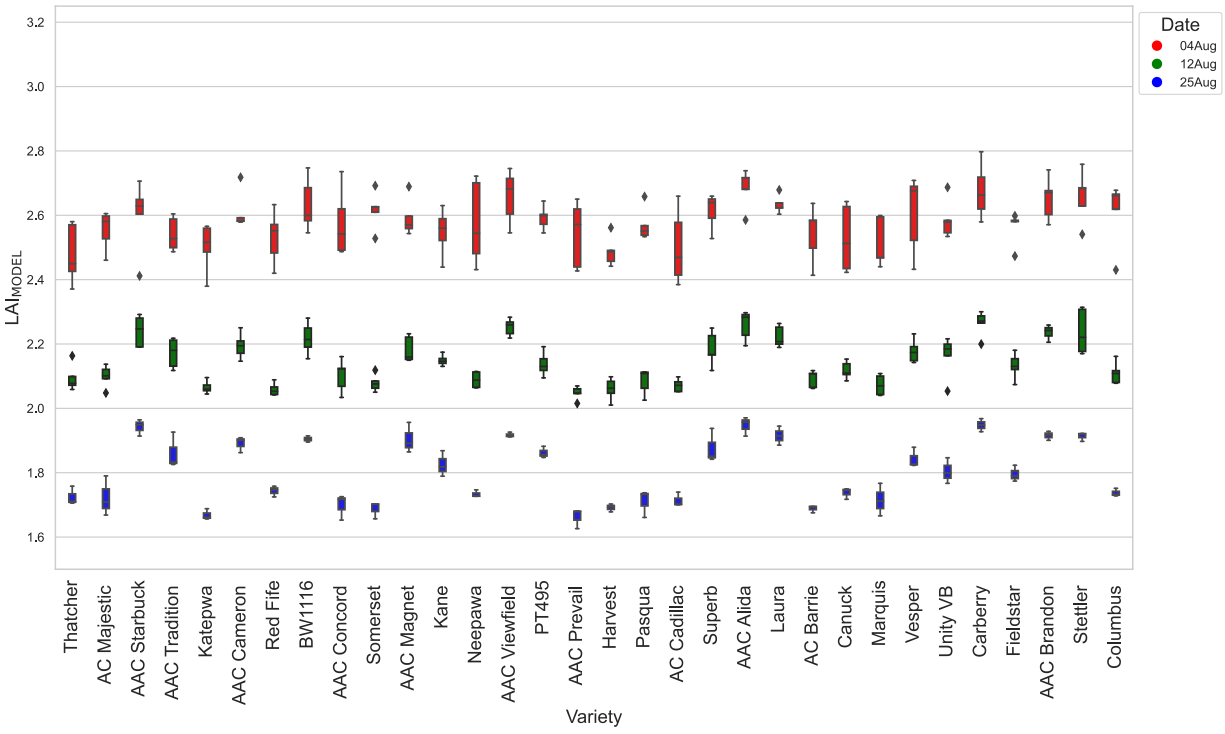

Figure 5.5: Relationship between the $\text{LAI}_{\text{MODEL}}$ values and varieties, with the exclusion of AAC Magnet, AAC Prevail, and Carberry, where the model incorporates date and canopy coverage as input parameters. For plots of each date, refer to Appendix A Figure A.4.

The reason that can be used to explain the improvement in findings that were made possible by removing specific varieties from the dataset is that the model underwent a reduction in complexity, leading to a simplified version. As a result, the overall relationship between date, canopy coverage, and LAI was more accurately depicted in the remaining data. However, even though the model exhibited improved performance after excluding three varieties, it was not selected as the preferred model. To enhance the research findings by considering the influence of variety, the decision was made to revert to the original dataset, encompassing all 32 varieties.

To incorporate variety into the analysis, clusters were formed. Initially, each possible pair of varieties was considered as the center of two clusters. Varieties were then incrementally added to both clusters. The evaluation of each cluster was based on adjusted R^2 values. The variety was assigned to the cluster that exhibited the most significant improvement in adjusted R^2, while it was removed from the other cluster. This process continued until every variety was assigned to a specific cluster. The entire procedure was repeated for every possible pair of varieties. Ultimately, for each possible variety pair, the adjusted R^2 values of the

created two clusters were compared. The pair of clusters with the highest sum of adjusted R^2 values was selected as the optimal set of clusters. Utilizing the previously stated method, the chosen clusters generated an adjusted R^2 value of 0.60 and an RMSE value of 0.23 (cluster 1, 29 varieties), and an adjusted R^2 value of 0.83 and an RMSE value of 0.19 (cluster 2, 3 varieties - AAC Concord, Laura, and AAC Brandon).

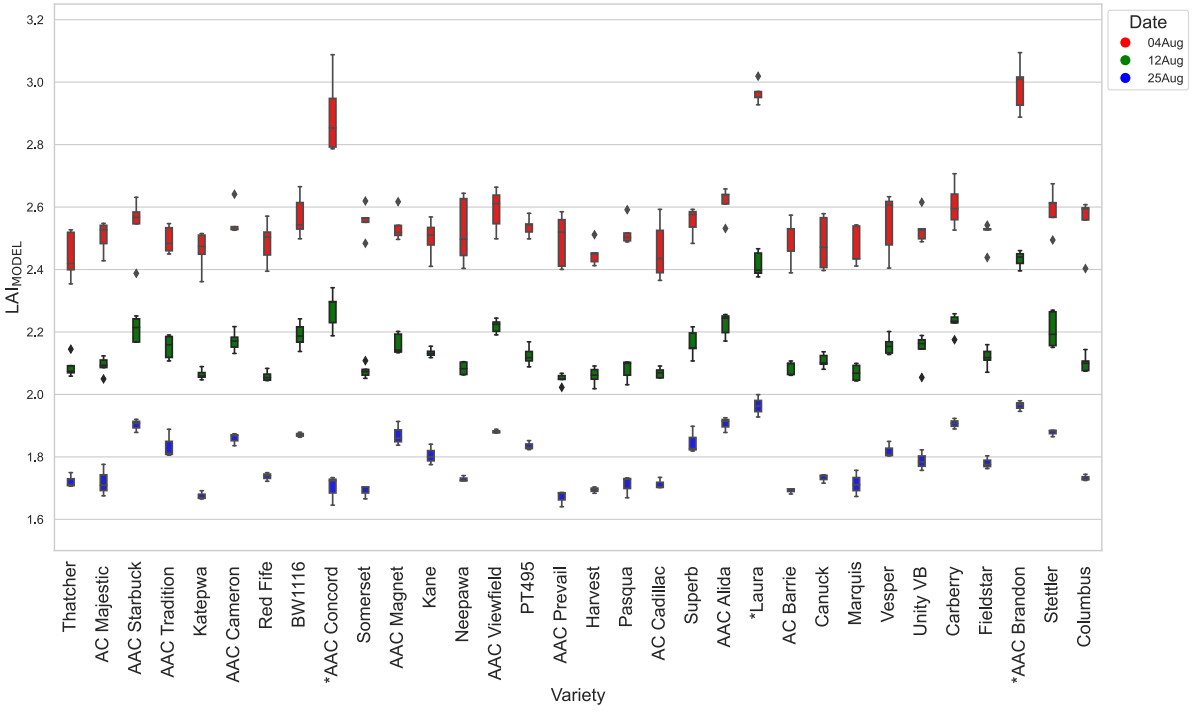

Figure 5.6: Relationship between the $\text{LAI}_{\text{MODEL}}$ values and varieties, utilizing the clustering method (brute-force approach) as described. Varieties marked with asterisks belong to the second cluster. For plots of each date, refer to Appendix A Figure A.5.

Figure 5.6 depicts the $\text{LAI}_{\text{MODEL}}$ values obtained from the model developed using the clustering method described. AAC Concord, Laura, and AAC Brandon clearly show higher $\text{LAI}_{\text{MODEL}}$ values in Figure 5.6, especially during the early dates. The fact that these three varieties were clustered separately from the other varieties may account for their slightly higher values than the others. With the exception of this distinction, Figure 5.6 shows a similar pattern to Figures 5.4 and 5.5, displaying a similar low variance as seen in those figures.

Following the initial selection of the clusters, an additional step was taken to assess whether further improvements could be made. A method was developed for this purpose, which involved examining the two kept clusters. The method systematically changed the cluster assignment of each variety, one by one, until

all varieties had been attempted in the alternative cluster. This procedure was repeated five times, with the order of the varieties randomized during each iteration. At the end of this process, the result either remained the same or exhibited improvement compared to the previous cluster assignment.

Upon implementing the improvement method, it was observed that it did not lead to any further enhancements over the first approach of creating clusters. Despite conducting the iterative procedure with randomized variety assignments and multiple repetitions, the results remained unchanged or did not show any improvement compared to the initial cluster configuration.

In the process of refining the model by excluding three specific varieties that impacted its data fitting capabilities, AAC Magnet, AAC Prevail, and Carberry were identified as the varieties for removal. Utilizing a brute force clustering method, two distinct clusters were formed, and within one of these clusters, AAC Concord, Laura, and AAC Brandon were grouped separately from the remaining varieties. The dissimilarity among these groups's varieties might be attributed to the way of the methodologies employed. In the case of excluding varieties, three specific varieties were removed from the dataset for each model. The model selection process involved comparing RMSE and adjusted R^2 values, with the optimal choice being determined by the model exhibiting the lowest RMSE and the highest adjusted R^2 value. In the brute-force clustering approach, the optimal set of clusters was determined by selecting the pair with the highest sum of adjusted R^2 values. To recap, the removal of varieties approach focused on individual model performance, with consideration given solely to the RMSE and adjusted R^2 values of one model, while the clustering method focused on the sum of adjusted R^2 values of models in two clusters.

As anticipated, Figure 5.6 demonstrates a comparable pattern to Figures 5.5, and 5.4, with a similar low variance observed in those figures. The variances, quantifying the dispersion of distribution and calculated using the Numpy library (NumPy.org, nd), for the datasets used to create Figure 5.4, Figure 5.5 and, Figure 5.6 are respectively 0.06, 0.07, 0.07. This outcome aligns with expectations, as these figures possess roughly equivalent prediction capabilities. The low variance in these figures may be attributed to the limited amount of data available and the narrow range of canopy coverage values, which are used as inputs for all the models represented by the figures. The average intra-variety difference differences of $\mathrm{LAI}_{\mathrm{MODEL}}$ values of the datasets utilized to generate Figures 5.4, 5.5 and, 5.6 are 0.09, 0.11 and, 0.1, respectively. These findings further corroborate the results obtained from the variance values. Consequently, the models represented by the figures are likely to predict LAI values that are precise and close to the mean of the test data, rather than exhibiting a wide range of variability.

Considering that models created using the clustering method outperformed other models in estimating LAI, the underlying reasons for this current clustering were investigated. In the present clustering approach, distinct clusters were formed for AAC Concord, Laura, and AAC Brandon varieties, whereas the remaining 29 varieties were grouped into a single cluster.

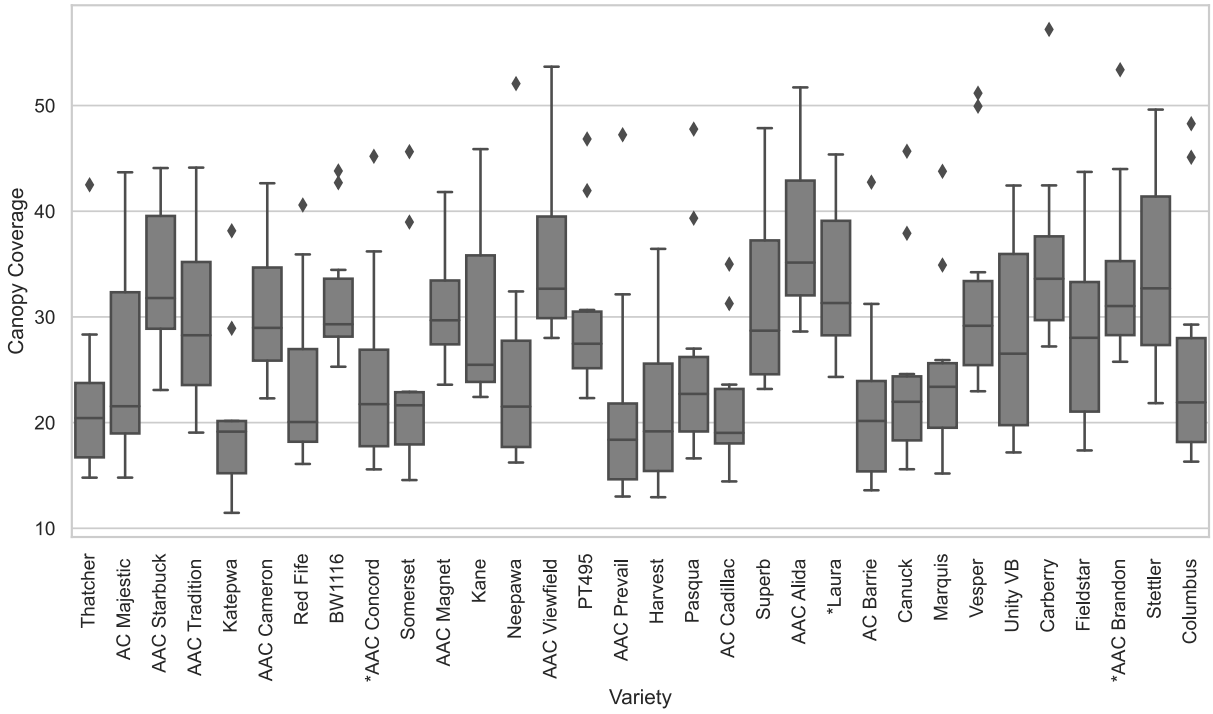

Figure 5.7: Relationship between the canopy coverage and varieties. Varieties marked with asterisks belong to the second cluster.

The potential influence of canopy coverage values on the current clustering pattern was investigated, and a boxplot depicting the relationship between canopy coverage and different varieties, specifically AAC Concord, Laura, and AAC Brandon, has been generated using data from the first two blocks of the field. In Figure 5.7, discerning the distinct mean and variability in the spread of data, particularly the interquartile ranges, among the three varieties in comparison to the others presents a challenge. The statistical analysis was conducted to examine whether the canopy coverage of these three varieties differs significantly from the other 29 varieties. Based on the p-value obtained from the analysis, it was observed that there is no statistically significant difference in canopy coverage among these three varieties compared to the remaining varieties.

To explore the existing clustering pattern more thoroughly, $\mathrm{LAI_{AZ}}$ value was introduced as an additional factor that could potentially exert influence. In Figure 5.8, generated from data extracted from the initial two blocks of the field, resembling the challenge encountered with canopy coverage, discerning the specific mean and variability in the data spread, particularly the interquartile ranges, among the three varieties in comparison to the rest is difficult. With a p-value of 0.0013, which is below the threshold of 0.05, it was evident that AAC Concord, Laura, and AAC Brandon exhibited a significant difference from the remaining varieties in terms of $\mathrm{LAI_{AZ}}$ values. Given that the $\mathrm{LAI_{AZ}}$ serves as the output for the clustering model, the

expectation was for this result to be observed.

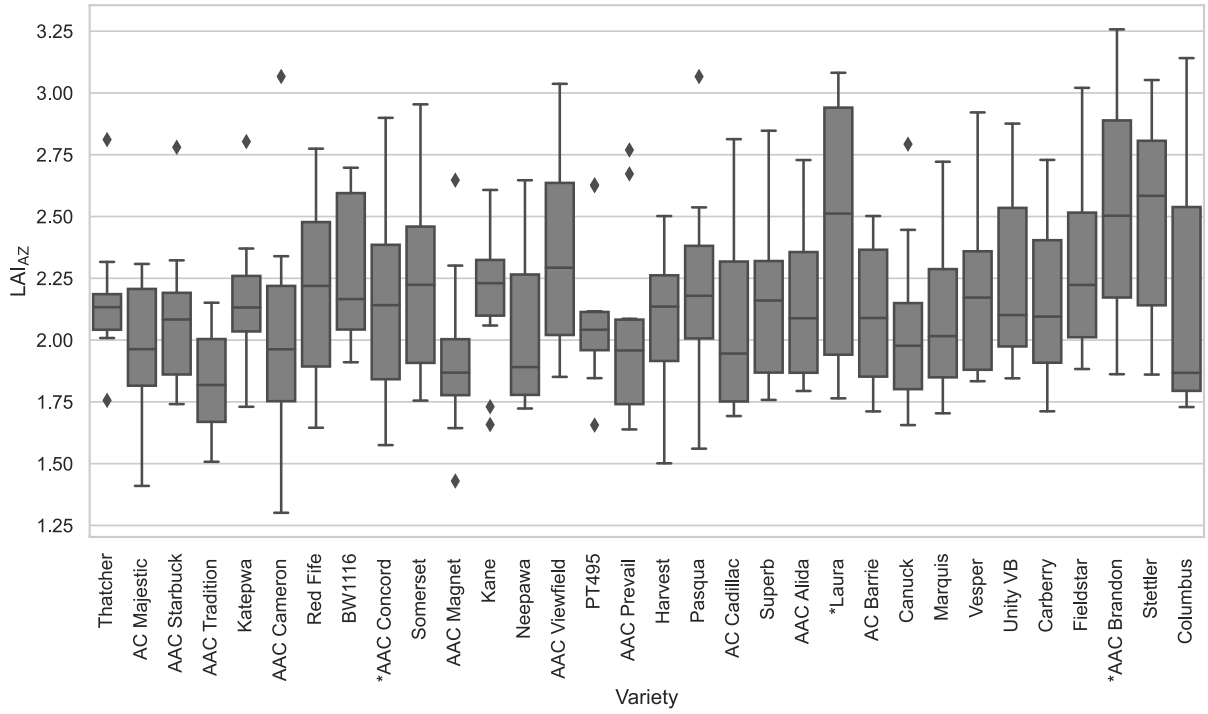

Figure 5.8: Relationship between the LAI_{AZ} values and varieties. Varieties marked with asterisks belong to the second cluster.

Due to the influence of LAI_{AZ} on the current clustering, further investigation was underway to examine how the behavior of these three varieties evolves as time progresses. In Figure 5.9, it is evident that AAC Concord, Laura, and AAC Brandon varieties exhibit lower LAI_{AZ} values after the initial data acquisition date. However, there is an increase in LAI_{AZ} values on the third date. Subsequently, following the third date, LAI_{AZ} values decrease for the remaining data acquisition dates. Despite not overlapping entirely, these varieties share a consistent pattern and behavior as time progresses. This observation suggested that one contributing factor to the current clustering was the consistent behavior of LAI_{AZ} values for AAC Concord, Laura, and AAC Brandon varieties over time.

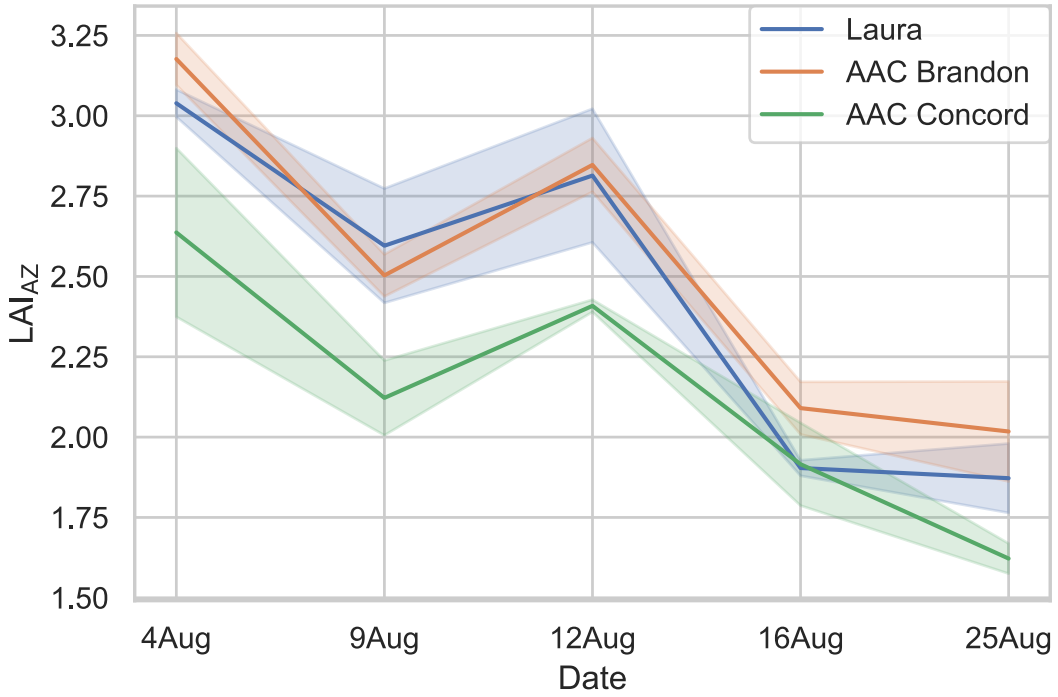

Figure 5.9: Relationship between the LAI_{AZ} values and Date for AAC Concord, Laura, and AAC Brandon varieties. The shading represents the confidence interval around the mean.

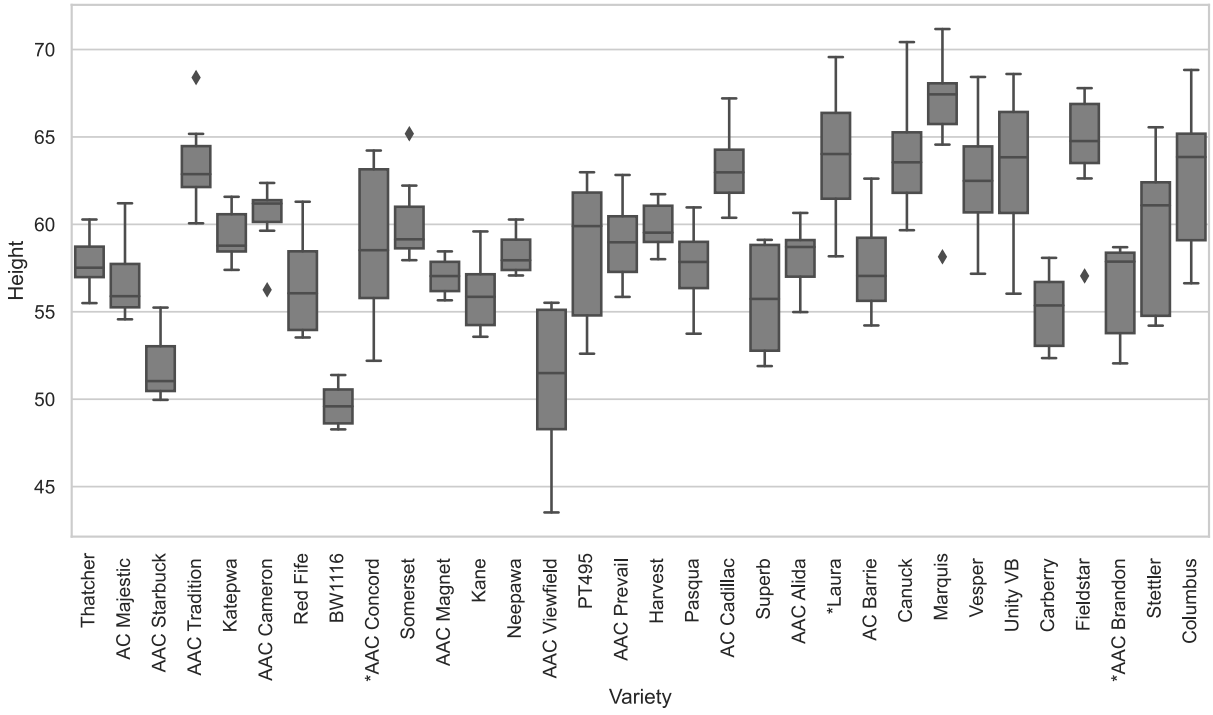

Figure 5.10: Relationship between the Height values and varieties. Varieties marked with asterisks belong to the second cluster.

To thoroughly investigate the existing clustering patterns, height was introduced as an additional variable to explore potential influences. In Figure 5.10, similar to the challenges faced in analyzing canopy coverage and LAI_{AZ}, discerning the specific mean and variability within the data spread, especially in terms of interquartile ranges, proves to be intricate when comparing the three varieties with the rest. Following comprehensive statistical analysis, it became evident that these three varieties exhibit a significant difference in height measurements compared to the remaining ones.

Given the observed influence of height on the current clustering, a more in-depth exploration was undertaken to understand how the behavior of the three varieties evolves over time. As depicted in Figure 5.11, noteworthy patterns emerged during the progression from the initial data acquisition date to the third, with Laura and AAC Concord exhibiting similar growth trends while Laura experienced a decrease. On the fourth date, all varieties displayed a consistent increase in height. However, by the last date, AAC Brandon and Laura demonstrated a decline, while AAC Concord maintained relative stability. This nuanced differentiation in behavior among the three varieties underscores the need for continued exploration, emphasizing that while similarities exist, a comprehensive understanding demands thorough investigation.

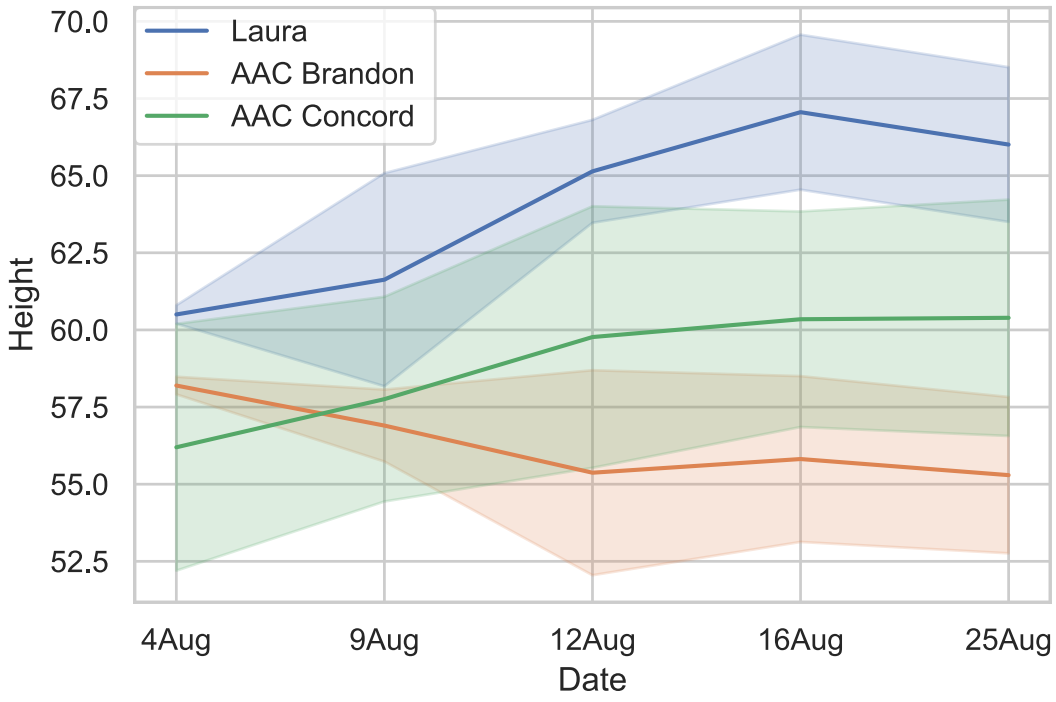

Figure 5.11: Relationship between the Height values and Date for AAC Concord, Laura, and AAC Brandon varieties.

For continued exploration, 5.12 has been generated, featuring three plots corresponding to AAC Brandon, Laura, and AAC Concord, respectively. Height values are represented on the x-axis, while five data acquisition dates stand on the y-axis. Each date presents two height values, with circle denoting Block 1 and square

denoting Block 2. The aim of this visualization was to uncover any consistent patterns or behaviors exhibited by these varieties across different blocks.

When attention was directed to Block 1, a decreasing trend in height across the dates was observed for AAC Brandon, while Laura and AAC Concord displayed an increasing trend. Notably, a significant height decrease on August 9 was experienced by Laura, potentially attributed to logging activities or other external factors. Shifting the focus to Block 2, AAC Brandon showed minimal height changes, maintaining a relatively stable height. In contrast, Laura and AAC Concord demonstrated an upward trend in height. Despite this examination, a conclusive understanding of whether similar behavior in terms of height values was shared by these three varieties remains elusive.

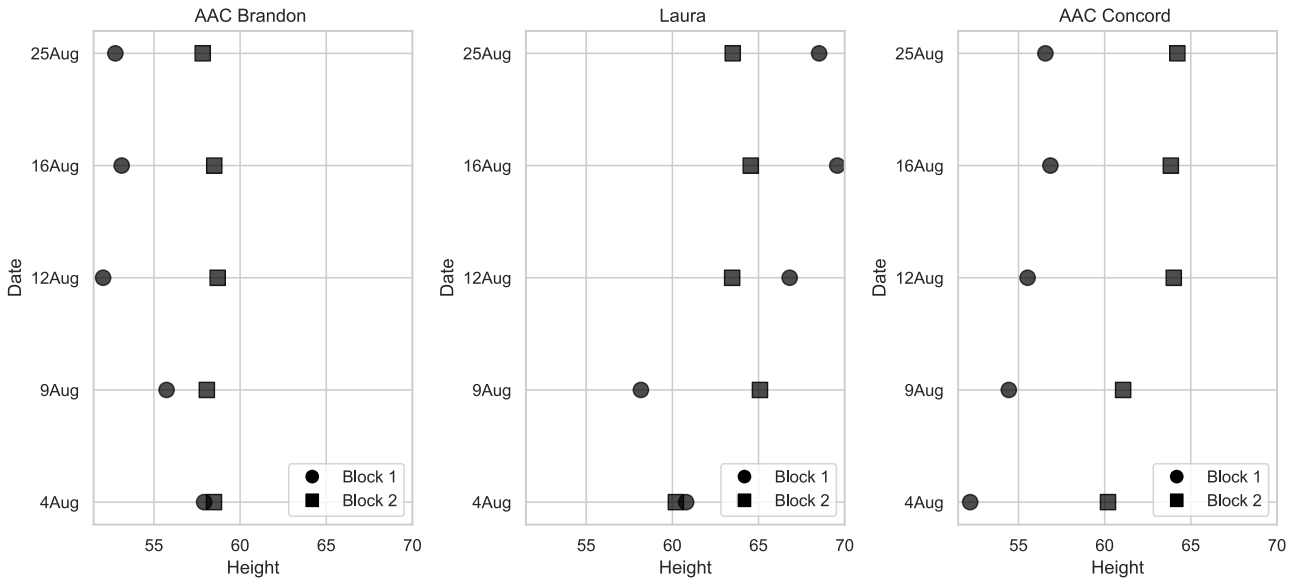

Figure 5.12: Growth patterns of AAC Brandon, Laura, and AAC Concord varieties over time, represented by distinctive geometric shapes in Block 1 (circle) and Block 2 (square).

In Figure 5.13, the relationship between LAI_{AZ} and Date, Canopy Coverage and LAI_{AZ}, and Canopy Coverage and Date across the first and second clusters are depicted. Higher LAI_{AZ} and Canopy Coverage values over time are observed in the second cluster. However, no noticeable difference in behavior between the first and second clusters is apparent when LAI_{AZ} is plotted against Canopy Coverage. Nevertheless, despite these insights, visually distinguishing between these two clusters is difficult.

Looking forward, a more comprehensive analysis with an expanded dataset could provide clearer insights into the underlying reasons for the current clustering of these varieties.

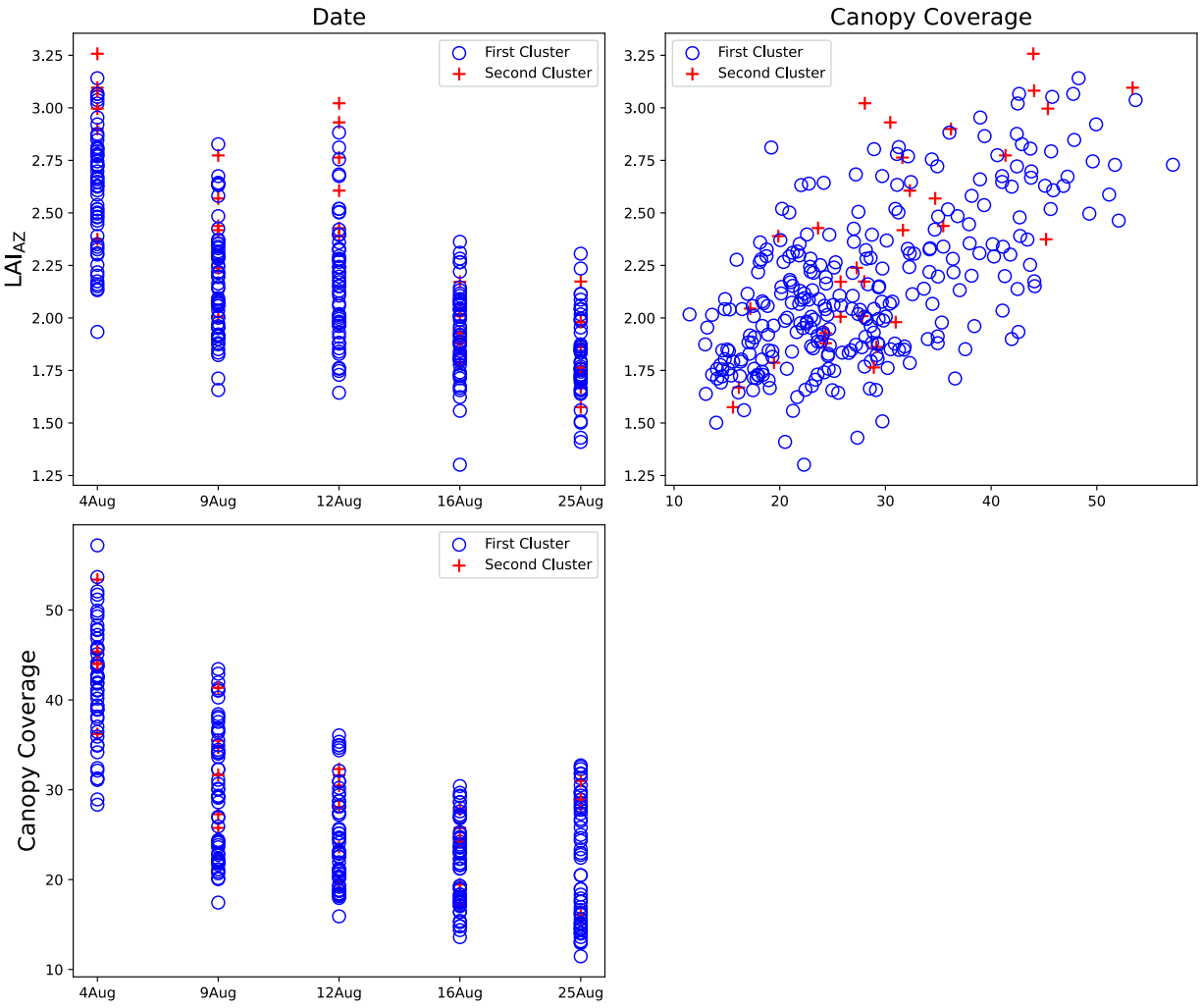

Figure 5.13: Relationship between Date, LAI_{AZ}, and Canopy Coverage for the first and second clusters.

To further improve the predictive capabilities of the model estimating LAI, it is essential to refine the assessment of canopy coverage. To ascertain canopy coverage accurately, an enhancement was introduced through the refinement of images via cropping for designated plots. The refinement process included cropping images into rectangular shapes centered around the plot, which deviates from the existing method lacking a centering and cropping procedure. Following this refinement, the images underwent processing within the existing pipeline, as in Section 4.4.1, to calculate canopy coverage from NIR images. Subsequently, the calculated canopy coverage values were integrated into an established pipeline to estimate LAI.

Table 5.7: Comparison of LAI prediction models with and without image cropping. CC denotes canopy coverage.

Model Input	**Adjusted R^2**	**RMSE**	**Adjusted R^2 (Cropped)**	**RMSE (Cropped)**
Canopy Coverage	0.50	0.29	0.51	0.29
Canopy Coverage & Date	0.58	0.26	0.59	0.26
Canopy Coverage & Date (utilizing brute-force approach clustering : two clusters)	0.60 & 0.83	0.23 & 0.19	0.60 & 0.83	0.23 & 0.19

In this investigation into the impact of image cropping on LAI prediction models, three distinct models were examined, each utilizing different input features as in Table 5.7. The first model, relying solely on Canopy Coverage, exhibited a slight improvement in model fit when image cropping was applied. The second model, incorporating both Canopy Coverage and Date as input features, also showed a minor enhancement in model performance with the introduction of cropping. Intriguingly, the third model, implementing a brute-force clustering approach with two clusters, did not change Adjusted R^2 and RMSE values; they were the same with cropping.

The results suggested a slight improvement in model performance following the implementation of image cropping. This enhancement was likely due to the practice of centering and cropping the plots, directing the analysis towards the region of interest within the image. It can diminish noise by adeptly filtering out extraneous elements in the original images. By concentrating on pertinent areas, cropped images potentially offered a more focused representation of canopy features compared to using the entire image as input.

Nevertheless, it is important to acknowledge that the observed improvement was modest, and there existed potential for further refinement. The current cropping technique, while beneficial, had its constraints. Enhancements to the cropping process could involve tailoring the approach to the unique characteristics of each plot. This customization may result in a more precise extraction of relevant information, thereby increasing the overall success of the model. Consequently, investigating alternative cropping strategies tailored to the specific characteristics of each plot may present a promising avenue for further optimization of the LAI prediction models.

6 Conclusions

In this research, line quantum sensors were employed to capture PAR readings within experimental plots. Utilizing these PAR readings alongside equations derived from commercial ceptometers, LAI_{PAR} values were calculated. LAI values served as the output for linear regression models, incorporating calculated input metrics for non-destructive LAI estimation. The metrics derived from imaging data included canopy coverage and height values, with height values determined using LiDAR data, while canopy coverage values were computed from NIR and visible light images. Date was used as a proxy for wheat canopy maturity. To assess model performance, RMSE and adjusted R^2 evaluation metrics were employed.

Three hypotheses were posited and tested within this study. Firstly, it was hypothesized that LAI_{PAR} values were significantly influenced by variations in the azimuth angle of the sun and time of day. Similar patterns between sun azimuth angle and LAI_{PAR} values across data acquisition dates were observed, and this effect was addressed through a data-driven correction, eliminating the impact of sun azimuth angle and time of day on LAI_{PAR} values. The research concluded that variations in the azimuth angle of the sun had a notable effect on LAI_{PAR} values.

The second hypothesis explored the accuracy of LAI calculations based on canopy coverage derived from NIR images compared to visible light images. Three models were developed, utilizing different inputs for LAI prediction: NIR image-based canopy coverage, visible light image-based canopy coverage considering only green pixels, and visible light image-based canopy coverage considering both green and yellow pixels. Results indicated that incorporating canopy coverage values from NIR images enhanced predictive accuracy, as evidenced by higher adjusted R^2 values and lower RMSE values. Moreover, canopy coverage from NIR images was assessed through thresholding, while machine learning was utilized to evaluate canopy coverage from visible light images. However, it's important to acknowledge that this approach introduces a limitation to the study, potentially leading to an inequitable comparison between the two methods.

Moreover, an investigation into the impact of incorporating height values as an input parameter in the LAI estimation model was undertaken. Because these values reached their maximum during data collection, it was observed that their inclusion did not enhance predictive power. In contrast, the introduction of a wheat canopy maturity proxy as an additional input parameter was shown to be beneficial, resulting in a reduction in RMSE and an increase in the adjusted R^2 value. This improvement indicated a noteworthy enhancement in the overall success of the model.

In the final hypothesis, the effectiveness of relying on a single model for LAI estimation through linear regression was questioned. Considering the diversity of 32 varieties in the dataset, a clustering method was

employed. The clustering outperformed the single model for estimating LAI, demonstrating that clustering varieties and developing unique models for each cluster yield better LAI estimation compared to a singular model encompassing all 32 varieties. This finding underscored the value of employing diverse models customized to specific variety clusters, thereby elevating the overall predictive performance of the model.

6.1 Limitation

The study has several limitations that influence its findings. Firstly, data collection spanned only one year, during the end of the growing season. To provide a more comprehensive understanding, data collection should extend over multiple years and cover the entirety of the growing seasons. Additionally, the PAR readings were conducted on just two blocks. A broader sampling across various blocks would enhance the robustness of the analysis.

Additionally, the clustering method employed in this study was brute-force. Exploring more sophisticated clustering methods could improve the accuracy of the results.

Furthermore, the assessment of canopy coverage differed between NIR and visible light images. While thresholding was utilized for NIR images, machine learning techniques were employed for visible light images. This discrepancy in methodology introduces a limitation.

Another potential limitation arises from the cropping strategy employed for NIR images in the LAI estimation model. The images were cropped into rectangular shapes centered around the plot, which may not fully account for the specific characteristics of each plot.

6.2 Future Work

In this research, the initial day of data collection was identified as day 1, and subsequent days were utilized as an indicator for assessing maturity. Alternatively, enhancing the accuracy of analysis can be achieved by incorporating more reliable maturity indicators that consider variations among plots, even on the same date. Furthermore, employing distinct models tailored to different maturity levels would contribute to refining prediction accuracy.

Beyond the established parameters of sun azimuth angle and time of day, there is a necessity for a thorough exploration of additional factors influencing LAI. Gaining insight into these factors will provide a more holistic understanding of crop growth dynamics and contribute to the creation of more resilient predictive models.

In this study, an approach is employed for clustering varieties through the utilization of the brute-force method. However, it is noteworthy to acknowledge that the integration of algorithms, such as the Expectation-Maximization algorithm, could be considered for further enhancement of the clustering process.

Furthermore, it is important to delve into the current clustering patterns of crop varieties and uncover the reasons behind these patterns. This inquiry will not only shed light on the diversity of crop responses but also pave the way for more informed and targeted analyses in future research.

An acknowledged limitation of this study was the reliance on data collected for only one year and the restriction of PAR readings to just two blocks. Future endeavors should prioritize expanding the dataset over multiple years to capture interannual variability and address potential anomalies. This expanded dataset will form the basis for improving the predictive capabilities of the models developed in this research, ensuring their robustness across varied growing seasons and environmental conditions.

References

Afrasiabian, Y., Noory, H., Mokhtari, A., Nikoo, M., Pourshakouri, F., and Haghighatmehr, P. (2021). Effects of spatial, temporal, and spectral resolutions on the estimation of wheat and barley leaf area index using multi- and hyper-spectral data (case study: Karaj, Iran). *Precision Agriculture*, 22.

Allen, L. H., J. (1974). Model of light penetration into a wide-row crop 1. *Agronomy Journal*, 66(1):41–47.

Armbrust, D. V. (1990). Rapid measurement of crop canopy cover. *Agronomy Journal*, 82(6):1170–1171.

Arumäe, T. and Lang, M. (2018). Estimation of canopy cover in dense mixed-species forests using airborne lidar data. *European Journal of Remote Sensing*, 51(1):132–141.

Aschonitis, V. G., Papamichail, D. M., Lithourgidis, A., and Fano, E. A. (2014). Estimation of leaf area index and foliage area index of rice using an indirect gravimetric method. *Communications in Soil Science and Plant Analysis*, 45(13):1726–1740.

Bar-Gera, H. (2017). The target parameter of adjusted r-squared in fixed-design experiments. *The American Statistician*, 71(2):112–119.

Battaglia, M., Cherry, M. L., Beadle, C. L., Sands, P. J., and Hingston, A. (1998). Prediction of leaf area index in eucalypt plantations: effects of water stress and temperature. *Tree Physiology*, 18(8–9):521–528.

Behera, S. K., Srivastava, P., Pathre, U. V., and Tuli, R. (2010). An indirect method of estimating leaf area index in Jatropha curcas L. using LAI-2000 plant canopy analyzer. *Agricultural and Forest Meteorology*, 150(2):307–311.

Berger, K., Atzberger, C., Danner, M., D'Urso, G., Mauser, W., Vuolo, F., and Hank, T. (2018). Evaluation of the PROSAIL model capabilities for future hyperspectral model environments: A review study. *Remote Sensing*, 10(2):85.

Bollinger, K. (2023). Leaf area index (LAI): The researcher's complete guide.

Boyd, N. S., Gordon, R., and Martin, R. C. (2002). Relationship between leaf area index and ground cover in potato under different management conditions. *Potato Research*, 45(2–4):117–129.

Bréda, N. J. J. (2003). Ground-based measurements of leaf area index: a review of methods, instruments and current controversies. *Journal of Experimental Botany*, 54(392):2403–2417.

Chattaraj, S., Chakraborty, D., Garg, R., Singh, R., Singh, G., Sehgal, V., Sahoo, R., Singh, S., Gupta, V., and Chand, D. (2011). Evaluating the effect of irrigation on crop evapotranspiration in wheat (Triticum aestivum L.) by combining conventional and remote sensing methods. *Journal of Agricultural Physics*, 11:35–52.

Chen, J. M. and Black, T. A. (1992). Defining leaf area index for non-flat leaves. *Plant, Cell & Environment*, 15(4):421–429.

Chicco, D., Warrens, M. J., and Jurman, G. (2021). The coefficient of determination R-squared is more informative than SMAPE, MAE, MAPE, MSE and RMSE in regression analysis evaluation. *PeerJ. Computer Science*, 7:e623.

Cifuentes, R., Van der Zande, D., Farifteh, J., Salas, C., and Coppin, P. (2014). Effects of voxel size and sampling setup on the estimation of forest canopy gap fraction from terrestrial laser scanning data. *Agricultural and Forest Meteorology*, 194:230–240.

Darvishzadeh, R., Skidmore, A., Schlerf, M., and Atzberger, C. (2008). Inversion of a radiative transfer model for estimating vegetation LAI and chlorophyll in a heterogeneous grassland. *Remote Sensing of Environment*, 112(5):2592–2604.

Decagon (2013). *AccuPAR PAR/LAI Ceptometer Model LP-80 Operator's Manual*. Decagon Devices, Inc.

Decagon (n.d.). *Beam Fraction Calculation in the LP80*. Decagon Devices, Inc.

Facchi, A., Baroni, G., Boschetti, M., and Gandolfi, C. (2010). Comparing optical and direct methods for leaf area index determination in a maize crop. *Journal of Agricultural Engineering*, 41(1):33.

Fei, Y., Jiulin, S., Hongliang, F., Zuofang, Y., Jiahua, Z., Yunqiang, Z., Kaishan, S., Zongming, W., and Maogui, H. (2012). Comparison of different methods for corn LAI estimation over northeastern china. *International Journal of Applied Earth Observation and Geoinformation: ITC Journal*, 18:462–471.

Firman, D. M. and Allen, E. J. (1989). Relationship between light interception, ground cover and leaf area index in potatoes. *The Journal of Agricultural Science*, 113(3):355–359.

Fleck, S., Niinemets, Ü., Cescatti, A., and Tenhunen, J. D. (2003). Three-dimensional lamina architecture alters light-harvesting efficiency in fagus: a leaf-scale analysis. *Tree Physiology*, 23(9):577–589.

Flénet, F., Kiniry, J. R., Board, J. E., Westgate, M. E., and Reicosky, D. C. (1996). Row spacing effects on light extinction coefficients of corn, sorghum, soybean, and sunflower. *Agronomy Journal*, 88(2):185–190.

Gao, B.-C., Montes, M. J., Davis, C. O., and Goetz, A. F. H. (2009). Atmospheric correction algorithms for hyperspectral remote sensing data of land and ocean. *Remote Sensing of Environment*, 113:S17–S24.

Gerrano, A. S., Adebola, P. O., Jansen van Rensburg, W. S., and Laurie, S. M. (2015). Genetic variability in cowpea (*vigna unguiculata* (l.) walp.) genotypes. *Suid-Afrikaanse Tydskrif Vir Plant En Grond [South African Journal of Plant and Soil]*, 32(3):165–174.

Gong, P., Pu, R., Biging, G. S., and Larrieu, M. R. (2003). Estimation of forest leaf area index using vegetation indices derived from hyperion hyperspectral data. *IEEE Transactions on Geoscience and Remote Sensing: A Publication of the IEEE Geoscience and Remote Sensing Society*, 41(6):1355–1362.

Guiné, R., Andrade, S., and Gonçalves, F. (2015). Physical-chemical properties of corema album (white crowberry or camarinha).

Hoff, P. D. (2009). Linear regression. In *Springer Texts in Statistics*, pages 149–170. Springer New York.

Hosoi, F. and Omasa, K. (2006). Voxel-based 3-D modeling of individual trees for estimating leaf area density using high-resolution portable scanning lidar. *IEEE Transactions on Geoscience and Remote Sensing: A Publication of the IEEE Geoscience and Remote Sensing Society*, 44(12):3610–3618.

Hsiao, T. C., Heng, L., Steduto, P., Rojas-Lara, B., Raes, D., and Fereres, E. (2009). AquaCrop—the FAO crop model to simulate yield response to water: III. parameterization and testing for maize. *Agronomy Journal*, 101(3):448–459.

Ikotun, A. M., Ezugwu, A. E., Abualigah, L., Abuhaija, B., and Heming, J. (2023). K-means clustering algorithms: A comprehensive review, variants analysis, and advances in the era of big data. *Information Sciences*, 622:178–210.

Jacquemoud, S., Verhoef, W., Baret, F., Bacour, C., Zarco-Tejada, P. J., Asner, G. P., François, C., and Ustin, S. L. (2009). PROSPECT+SAIL models: A review of use for vegetation characterization. *Remote Sensing of Environment*, 113:S56–S66.

Jarquin, D., Howard, R., Xavier, A., and Das Choudhury, S. (2018). Increasing predictive ability by modeling interactions between environments, genotype and canopy coverage image data for soybeans. *Agronomy (Basel, Switzerland)*, 8(4):51.

Jay, S., Maupas, F., Bendoula, R., and Gorretta, N. (2017). Retrieving LAI, chlorophyll and nitrogen contents in sugar beet crops from multi-angular optical remote sensing: Comparison of vegetation indices and PROSAIL inversion for field phenotyping. *Field Crops Research*, 210:33–46.

Jensen, A. (1980). Seasonal changes in near infrared reflectance ratio and sanding crop biomass in a salt marsh community dominated by *Halimione portulacoides* (l.) aellen. *The New Phytologist*, 86(1):57–67.

Jimenez-Berni, J. A., Deery, D. M., Rozas-Larraondo, P., Condon, A. G., Rebetzke, G. J., James, R. A., Bovill, W. D., Furbank, R. T., and Sirault, X. R. R. (2018). High throughput determination of plant height, ground cover, and above-ground biomass in wheat with LiDAR. *Frontiers in Plant Science*, 9.

Kang, Y., Özdoğan, M., Zipper, S., Román, M., Walker, J., Hong, S., Marshall, M., Magliulo, V., Moreno, J., Alonso, L., Miyata, A., Kimball, B., and Loheide, S. (2016). How universal is the relationship between remotely sensed vegetation indices and crop leaf area index? A global assessment. *Remote Sensing*, 8(7):597.

Knipling, E. B. (1970). Physical and physiological basis for the reflectance of visible and near-infrared radiation from vegetation. *Remote Sensing of Environment*, 1(3):155–159.

Korhonen, L., Korpela, I., Heiskanen, J., and Maltamo, M. (2011). Airborne discrete-return LIDAR data in the estimation of vertical canopy cover, angular canopy closure and leaf area index. *Remote Sensing of Environment*, 115(4):1065–1080.

Leach, L. F. and Henson, R. K. (2007). The use and impact of adjusted R^2 effects in published regression research. *Multiple Linear Regression Viewpoints*, 33(1):1–11.

Lee, K.-S., Cohen, W. B., Kennedy, R. E., Maiersperger, T. K., and Gower, S. T. (2004). Hyperspectral versus multispectral data for estimating leaf area index in four different biomes. *Remote Sensing of Environment*, 91(3–4):508–520.

Li, F., Peng, Y., Zhang, D., Yang, G., Fang, K., Wang, G., Wang, J., Yu, J., Zhou, G., and Yang, Y. (2019). Leaf area rather than photosynthetic rate determines the response of ecosystem productivity to experimental warming in an alpine steppe. *Journal of Geophysical Research. Biogeosciences*, 124(7):2277–2287.

LI-COR (2021). *LAI-2200C Plant Canopy Analyzer Instruction Manual*. LI-COR, Inc.

LI-COR, Inc. (2015). *Terrestrial Quantum Sensors Instruction Manual*.

Lim, K., Treitz, P., Wulder, M., St-Onge, B., and Flood, M. (2003). LiDAR remote sensing of forest structure. *Progress in Physical Geography*, 27(1):88–106.

Liu, K., Zhou, Q.-B., Wu, W.-B., Xia, T., and Tang, H.-J. (2016). Estimating the crop leaf area index using hyperspectral remote sensing. *Journal of Integrative Agriculture*, 15(2):475–491.

López-Lozano, R. and Casterad, M. A. (2013). Comparison of different protocols for indirect measurement of leaf area index with ceptometers in vertically trained vineyards: Leaf area index measurement with ceptometers. *Australian Journal of Grape and Wine Research*, 19(1):116–122.

Madec, S., Baret, F., de Solan, B., Thomas, S., Dutartre, D., Jezequel, S., Hemmerlé, M., Colombeau, G., and Comar, A. (2017). High-throughput phenotyping of plant height: Comparing unmanned aerial vehicles and ground LiDAR estimates. *Frontiers in Plant Science*, 8.

Mananze, S., Pôças, I., and Cunha, M. (2018). Retrieval of maize leaf area index using hyperspectral and multispectral data. *Remote Sensing*, 10(12):1942.

Michalsky, J. J. (1988). The astronomical almanac's algorithm for approximate solar position (1950–2050). *Solar Energy (Phoenix, Ariz.)*, 40(3):227–235.

Monteith, J. L. and Moss, C. J. (1977). Climate and the efficiency of crop production in Britain. *Philosophical Transactions of the Royal Society of London*, 281(980):277–294.

Nielsen, D. C., Miceli-Garcia, J. J., and Lyon, D. J. (2012). Canopy cover and leaf area index relationships for wheat, triticale, and corn. *Agronomy Journal*, 104(6):1569–1573.

Niinemets, Ü. (2010). A review of light interception in plant stands from leaf to canopy in different plant functional types and in species with varying shade tolerance. *Ecological Research*, 25(4):693–714.

Norman, J. M. (1988). Crop canopy photosynthesis and conductance from leaf measurements. Workshop prepared for LI-COR, Inc., Lincoln, Nebr., 1988. (From Welles, J. M., Some indirect methods of estimating canopy structure, in Instrumentation for Studying Vegetation Canopies for Remote Sensing in Optical and Thermal Infrared Region, edited by N. S. Goel and J. M. Norman, Remote Sens. Rev., 5(1), 31-43, 1988.).

NumPy.org (n.d.). Numpy.Var — NumPy v1.26 manual. `https://numpy.org/doc/stable/reference/generated/numpy.var.html`. Accessed April 28, 2024.

Open3DKey (n.d.). Open3D: A modern library for 3D data processing.

Otsu, N. (1979). A threshold selection method from gray-level histograms. *IEEE Transactions on Systems, Man, and Cybernetics*, 9(1):62–66.

Peduzzi, A., Wynne, R. H., Fox, T. R., Nelson, R. F., and Thomas, V. A. (2012). Estimating leaf area index in intensively managed pine plantations using airborne laser scanner data. *Forest Ecology and Management*, 270:54–65.

Pinilla, J. and Negrín, M. (2021). Non-parametric generalized additive models as a tool for evaluating policy interventions. *Mathematics*, 9(4):299.

Pokovai, K. and Fodor, N. (2019). Adjusting ceptometer data to improve leaf area index measurements. *Agronomy (Basel, Switzerland)*, 9(12):866.

Purcell, L. C. (2000). Soybean canopy coverage and light interception measurements using digital imagery. *Crop Science*, 40(3):834–837.

Purkis, S. J. and Brock, J. C. (2013). LiDAR overview. In *Coral Reef Remote Sensing*, pages 115–143. Springer Netherlands.

pyGAM documentation (n.d.). LinearGAM — pyGAM documentation. Retrieved March 26, 2024.

Qin, J., Chao, K., Kim, M. S., Lu, R., and Burks, T. F. (2013). Hyperspectral and multispectral imaging for evaluating food safety and quality. *Journal of Food Engineering*, 118(2):157–171.

Rahman, M., Islam, M., Islam, T., and Karim, M. (2014). Dry matter accumulation, leaf area index and yield responses of wheat under different levels of nitrogen. *Bangladesh J. Agriculturist*, 7:27–32.

Raj, R., Walker, J. P., Pingale, R., Nandan, R., Naik, B., and Jagarlapudi, A. (2021). Leaf area index estimation using top-of-canopy airborne RGB images. *International Journal of Applied Earth Observation and Geoinformation: ITC Journal*, 96:102282.

Ranson, K., Daughtry, C., Biehl, L., and Bauer, M. (1985). Sun-view angle effects on reflectance factors of corn canopies. *Remote Sensing of Environment*, 18(2):147–161.

Roosjen, P. P. J., Brede, B., Suomalainen, J. M., Bartholomeus, H. M., Kooistra, L., and Clevers, J. G. P. W. (2018). Improved estimation of leaf area index and leaf chlorophyll content of a potato crop using multi-angle spectral data – potential of unmanned aerial vehicle imagery. *International Journal of Applied Earth Observation and Geoinformation: ITC Journal*, 66:14–26.

Rosati, A. (2001). Estimating canopy light interception and absorption using leaf mass per unit leaf area in Solanum melongena. *Annals of Botany*, 88(1):101–109.

Ross, C. W., Loudermilk, E. L., Skowronski, N., Pokswinski, S., Hiers, J. K., and O'Brien, J. (2022). LiDAR voxel-size optimization for canopy gap estimation. *Remote Sensing*, 14(5):1054.

Roth, L., Aasen, H., Walter, A., and Liebisch, F. (2018). Extracting leaf area index using viewing geometry effects—A new perspective on high-resolution unmanned aerial system photography. *ISPRS Journal of Photogrammetry and Remote Sensing: Official Publication of the International Society for Photogrammetry and Remote Sensing (ISPRS)*, 141:161–175.

Roth, L. and Streit, B. (2018). Predicting cover crop biomass by lightweight UAS-based RGB and NIR photography: an applied photogrammetric approach. *Precision Agriculture*, 19(1):93–114.

Royo, S. and Ballesta-Garcia, M. (2019). An overview of lidar imaging systems for autonomous vehicles. *Applied Sciences (Basel, Switzerland)*, 9(19):4093.

Saiyed, I. M., Bullock, P. R., Sapirstein, H. D., Finlay, G. J., and Jarvis, C. K. (2009). Thermal time models for estimating wheat phenological development and weather-based relationships to wheat quality. *Canadian Journal of Plant Science*, 89(3):429–439.

Salter, W. T., Gilbert, M. E., and Buckley, T. N. (2018). Time-dependent bias in instantaneous ceptometry caused by row orientation. *The Plant Phenome Journal*, 1(1):1–10.

Schmidt, A. F. and Finan, C. (2018). Linear regression and the normality assumption. *Journal of Clinical Epidemiology*, 98:146–151.

Schroeder, L. D., Sjoquist, D. L., and Stephan, P. E. (1986). *Understanding Regression Analysis: An Introductory Guide*. Sage Publications.

Scikit-Learn (n.d.). sklearn.model_selection.train_test_split. Retrieved April 26, 2024.

Shaykewich, C. F. (1995). An appraisal of cereal crop phenology modelling. *Canadian Journal of Plant Science*, 75(2):329–341.

Stewart, A. M., Edmisten, K. L., Wells, R., and Collins, G. D. (2007). Measuring canopy coverage with digital imaging. *Communications in Soil Science and Plant Analysis*, 38(7–8):895–902.

Stewart, D. W., Costa, C., Dwyer, L. M., Smith, D. L., Hamilton, R. I., and Ma, B. L. (2003). Canopy structure, light interception, and photosynthesis in maize. *Agronomy Journal*, 95(6):1465–1474.

Thenkabail, P. S., Enclona, E. A., Ashton, M. S., and Van Der Meer, F. (2004). Accuracy assessments of hyperspectral waveband performance for vegetation analysis applications. *Remote Sensing of Environment*, 91(3–4):354–376.

Tian, L. and Qu, Y. (2023). Assessing factors that affect the estimation of a canopy's gap fraction and extinction coefficient using discrete airborne LiDAR data. *IEEE Transactions on Geoscience and Remote Sensing*, 61(Art no. 5701814):1–14.

Walker, G. K. (1989). Model for operational forecasting of Western Canada wheat yield. *Agricultural and Forest Meteorology*, 44(3–4):339–351.

Walter, J. D. C., Edwards, J., McDonald, G., and Kuchel, H. (2019). Estimating biomass and canopy height with LiDAR for field crop breeding. *Frontiers in Plant Science*, 10.

Wang, K., Zhou, H., Wang, B., Jian, Z., Wang, F., Huang, J., Nie, L., Cui, K., and Peng, S. (2013). Quantification of border effect on grain yield measurement of hybrid rice. *Field Crops Research*, 141:47–54.

Wang, X., Singh, D., Marla, S., Morris, G., and Poland, J. (2018). Field-based high-throughput phenotyping of plant height in sorghum using different sensing technologies. *Plant Methods*, 14(1).

Wang, Y. and Fang, H. (2020). Estimation of LAI with the LiDAR technology: A review. *Remote Sensing*, 12(20):3457.

White, M. A., Asner, G. P., Nemani, R. R., Privette, J. L., and Running, S. W. (2000). Measuring fractional cover and leaf area index in arid ecosystems. *Remote Sensing of Environment*, 74(1):45–57.

Wilhelm, W. W., Ruwe, K., and Schlemmer, M. R. (2000). Comparison of three leaf area index meters in a corn canopy. *Crop Science*, 40(4):1179–1183.

Yang, P., Wu, W.-B., Tang, H.-J., Zhou, Q.-B., Zou, J.-Q., and Zhang, L. (2007). Mapping spatial and temporal variations of leaf area index for winter wheat in north China. *Agricultural Sciences in China*, 6(12):1437–1443.

Yuan, Y., Wang, X., Yin, F., and Zhan, J. (2013). Examination of the quantitative relationship between vegetation canopy height and LAI. *Advances in Meteorology*, 2013:1–6.

Zhang, D., Liu, J., Ni, W., Sun, G., Zhang, Z., Liu, Q., and Wang, Q. (2019). Estimation of forest leaf area index using height and canopy cover information extracted from unmanned aerial vehicle stereo imagery. *IEEE Journal of Selected Topics in Applied Earth Observations and Remote Sensing*, 12(2):471–481.

Zhang, Q., Xiao, X., Braswell, B., Linder, E., Baret, F., and Moore III, B. (2005). Estimating light absorption by chlorophyll, leaf and canopy in a deciduous broadleaf forest using MODIS data and a radiative transfer model. *Remote Sensing of Environment*, 99(3):357–371.

Zhao, D., Huang, L., Li, J., and Qi, J. (2007). A comparative analysis of broadband and narrowband derived vegetation indices in predicting LAI and CCD of a cotton canopy. *ISPRS Journal of Photogrammetry and Remote Sensing: Official Publication of the International Society for Photogrammetry and Remote Sensing (ISPRS)*, 62(1):25–33.

Zheng, H., Cheng, T., Li, D., Zhou, X., Yao, X., Tian, Y., Cao, W., and Zhu, Y. (2018). Evaluation of RGB, color-infrared and multispectral images acquired from unmanned aerial systems for the estimation of nitrogen accumulation in rice. *Remote Sensing*, 10(6):824.

Appendix A

Figures

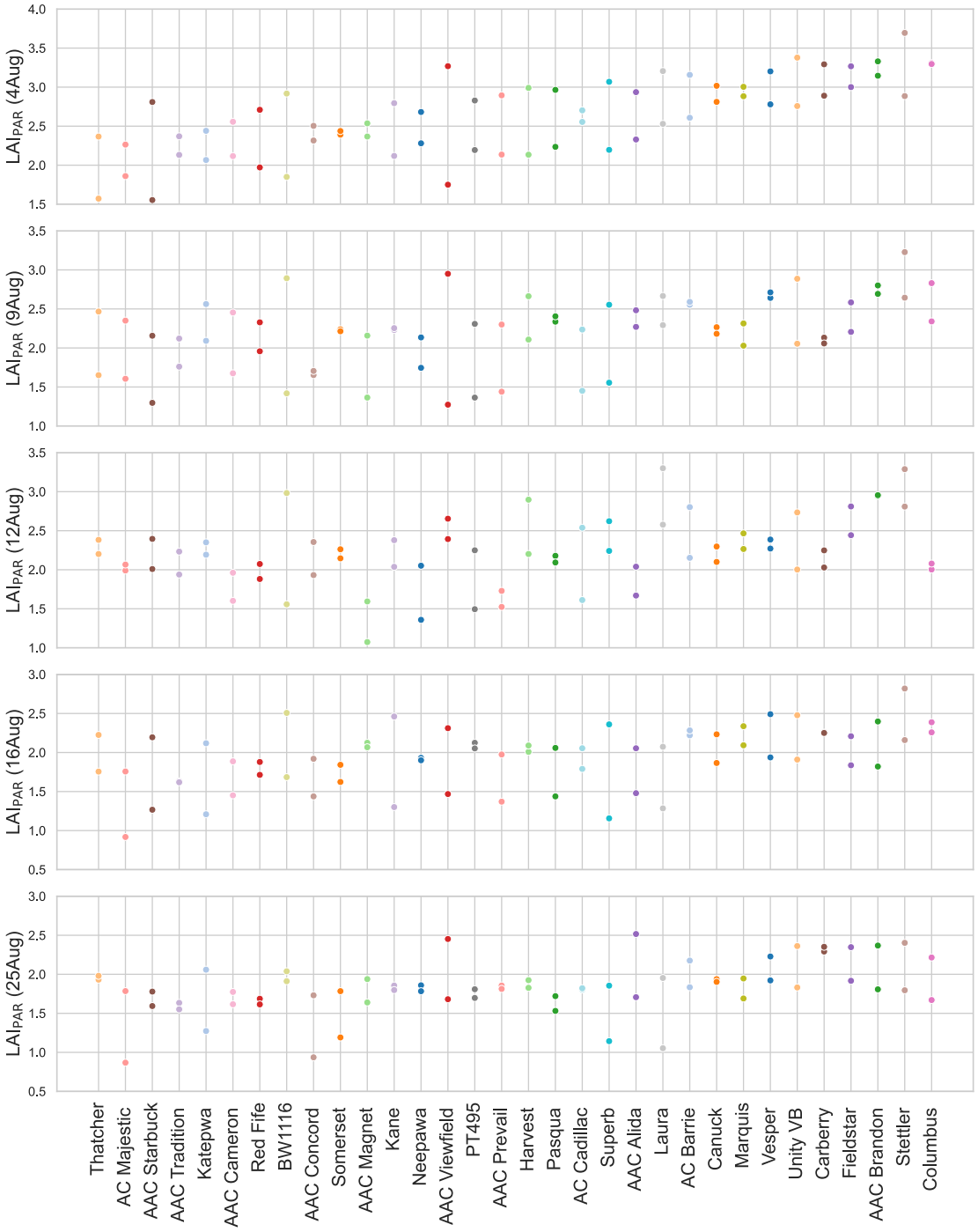

Figure A.1: Relationship between the LAI_{PAR} values and varieties.

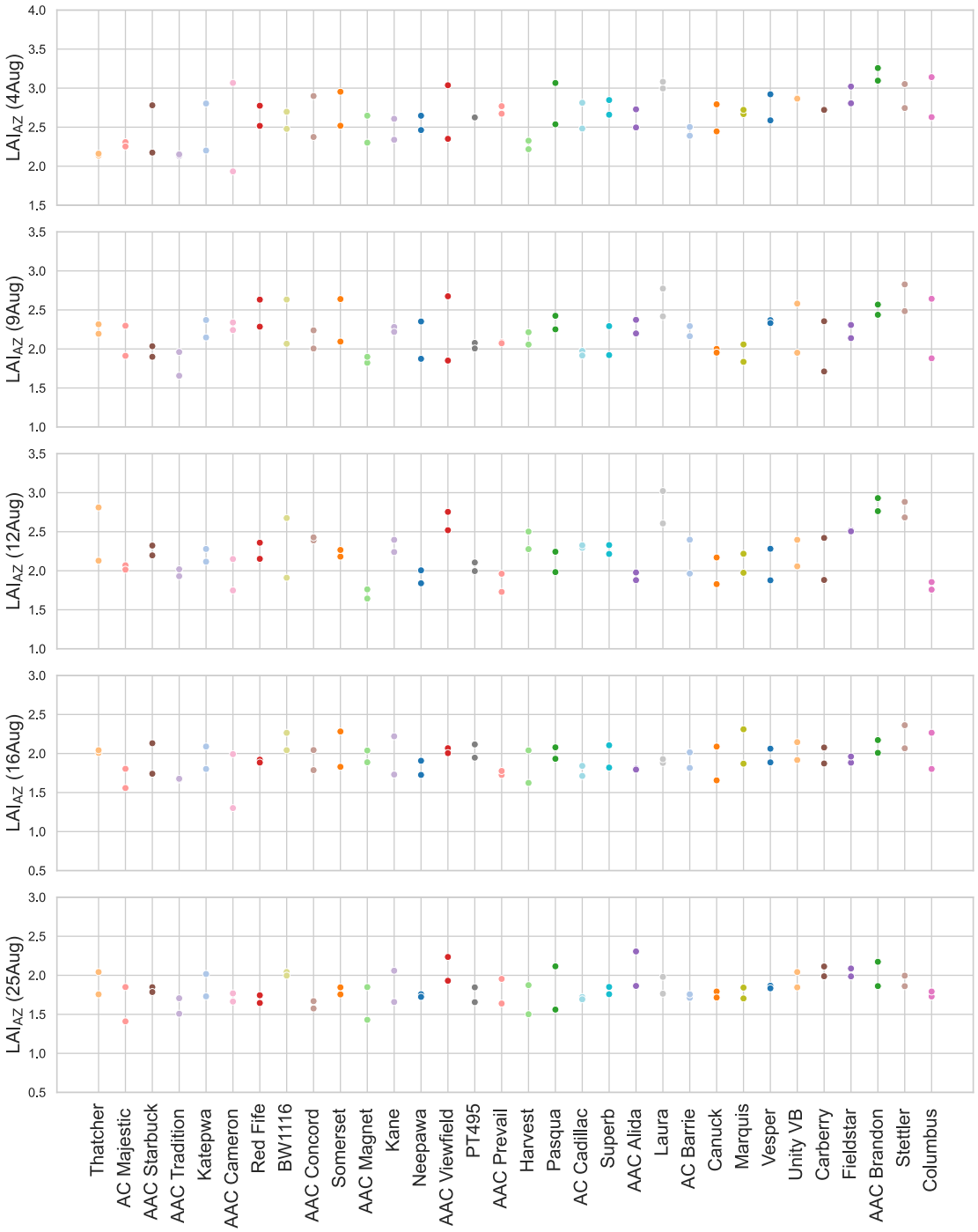

Figure A.2: Relationship between the $\mathrm{LAI_{AZ}}$ values and varieties.

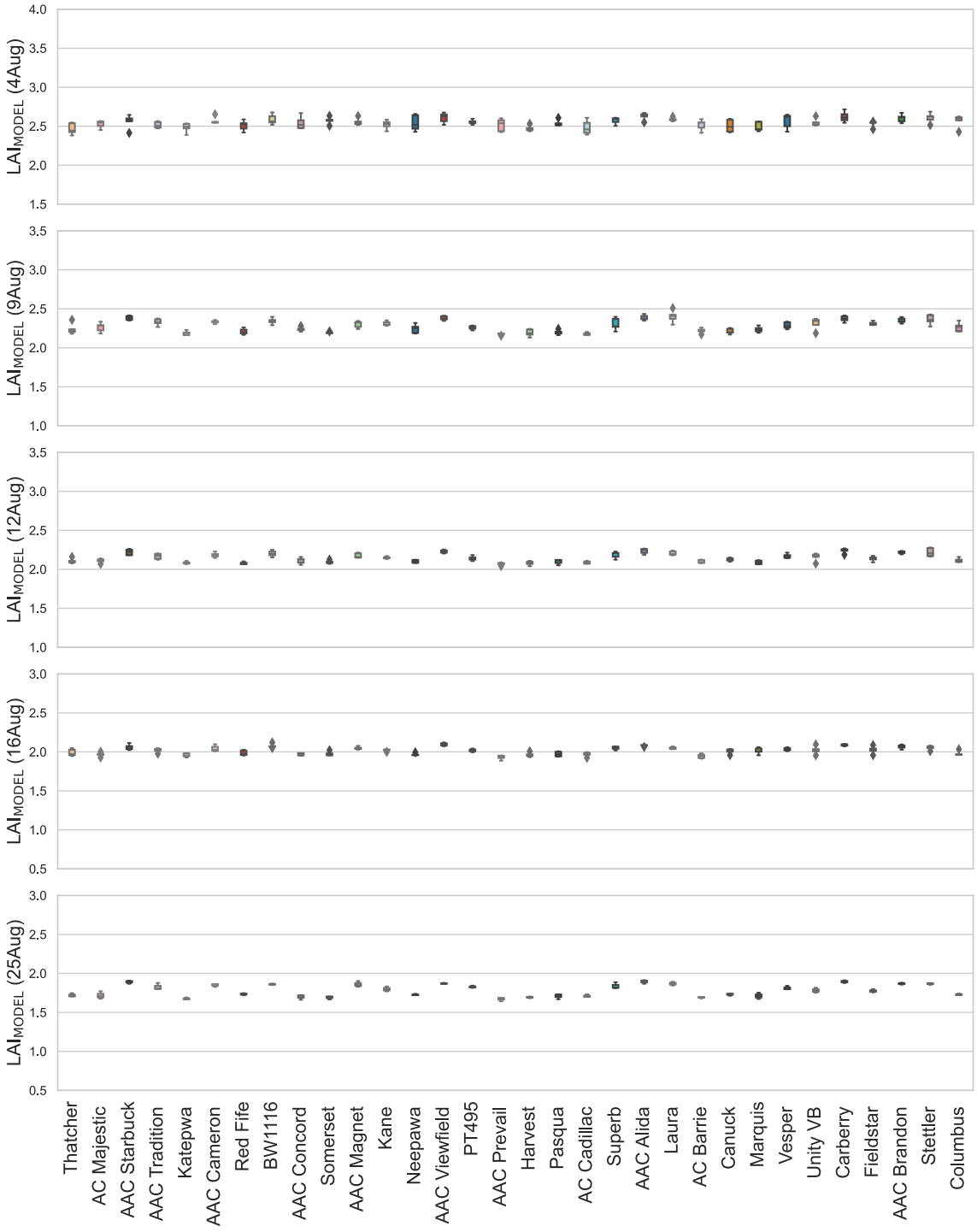

Figure A.3: Relationship between the $\mathrm{LAI}_{\mathrm{MODEL}}$ values and varieties, where the model incorporates date and canopy coverage as input parameters.

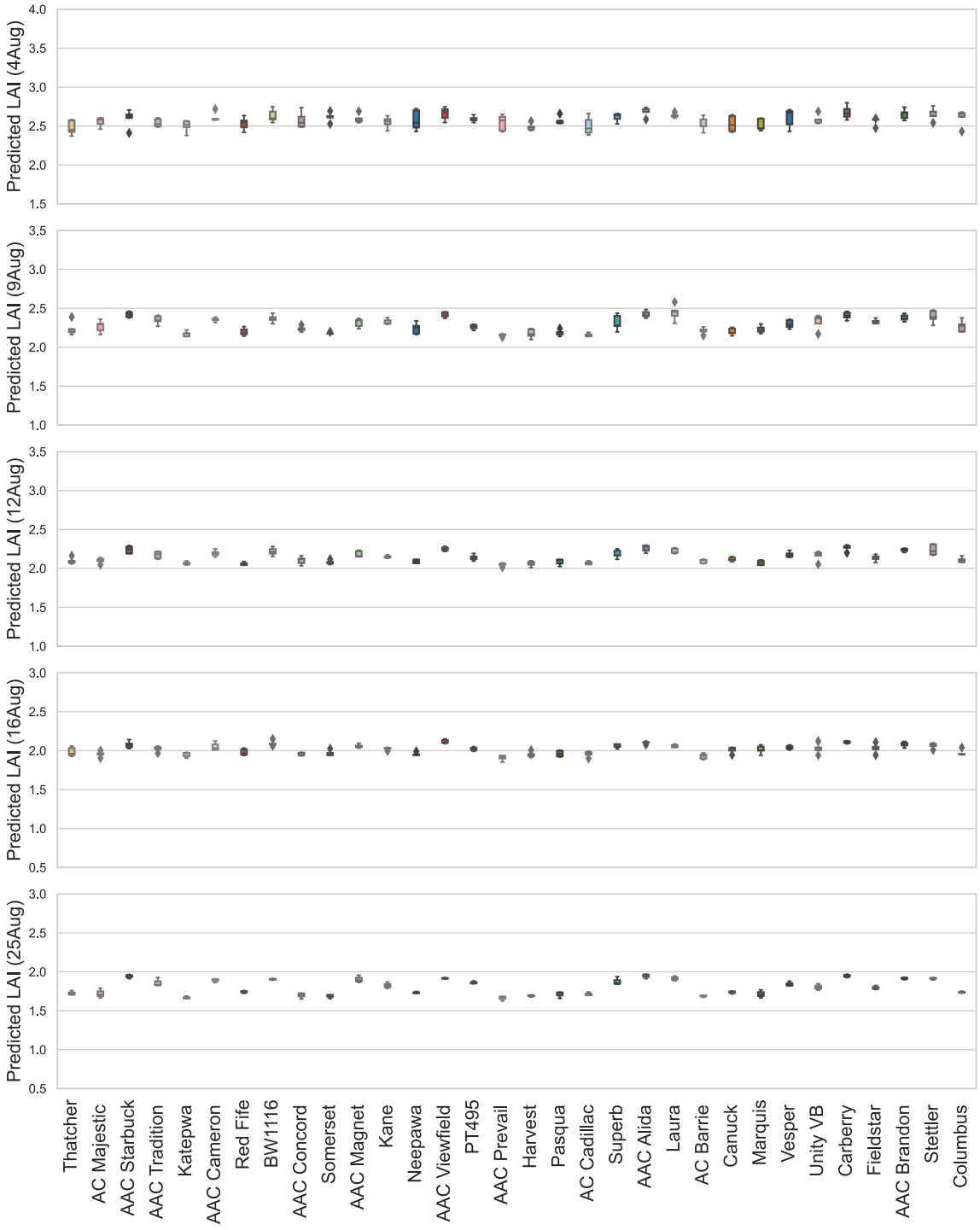

Figure A.4: Relationship between the $\text{LAI}_{\text{MODEL}}$ values and varieties, with the exclusion of AAC Magnet, AAC Prevail, and Carberry, where the model incorporates date and canopy coverage as input parameters.

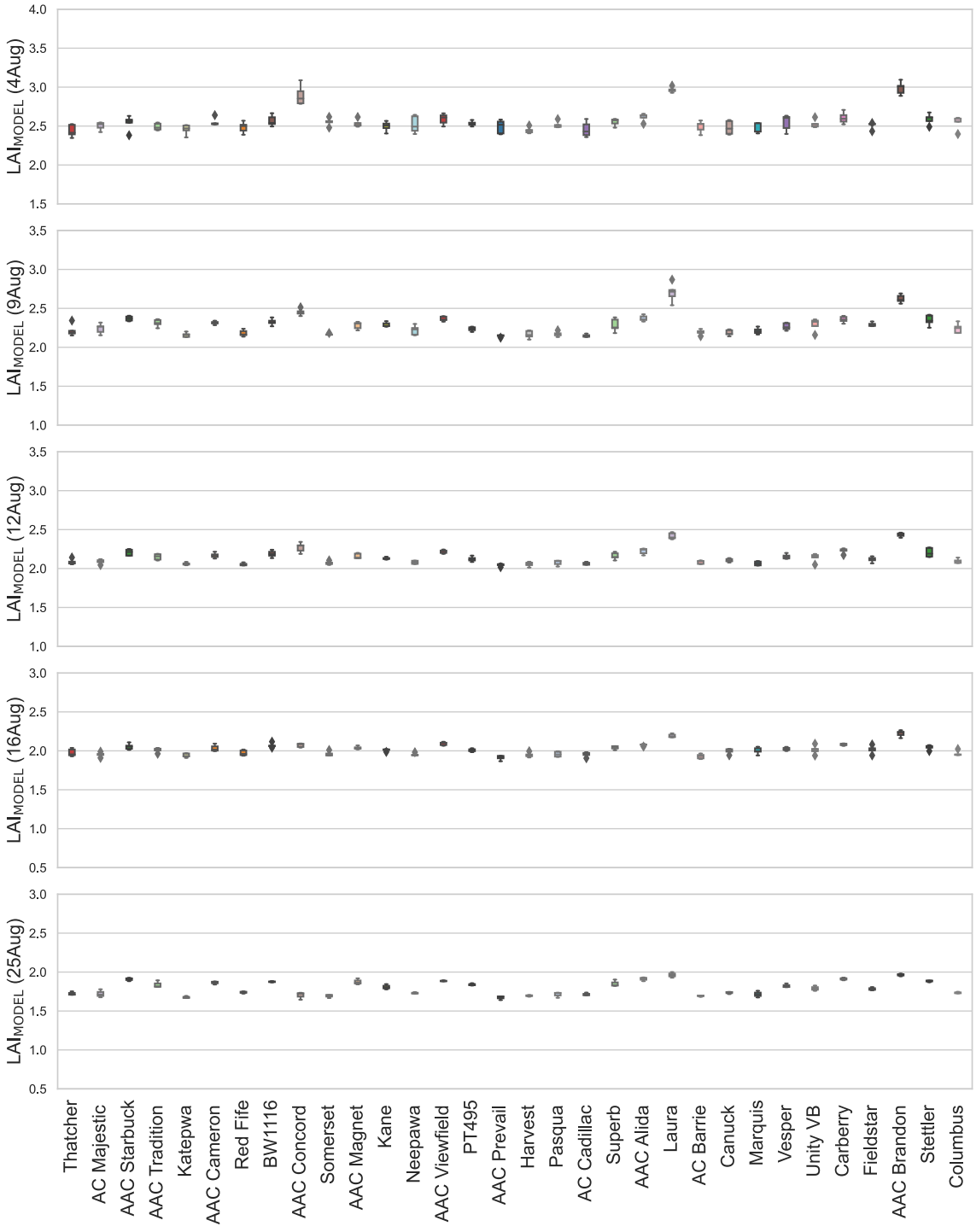

Figure A.5: Relationship between the $\mathrm{LAI}_{\mathrm{MODEL}}$ values and varieties, utilizing the clustering method.

Table A.1: Model parameters and evaluation metrics of the developed models, with corresponding sections indicated.

Input Parameter(s)	Output Parameter	Coefficient(s)	Intercept	Adjusted R^2	RMSE	Section
NIR CC	LAI_{PAR}	0.024	1.472	0.390	0.406	5.2.1
NIR CC	LAI_{AZ}	0.023	1.498	0.501	0.287	5.2.1
L*a*b* Vegetation CC	LAI_{AZ}	-0.005	2.256	-0.0373	0.413	5.2.2
L*a*b* Vegetation + Senescent CC	LAI_{AZ}	-0.005	2.468	0.009	0.404	5.2.2
Height	LAI_{AZ}	0.008	1.661	-0.077	0.421	5.2.3
Height & NIR CC	LAI_{AZ}	0.023 & 0.010	0.910	0.467	0.295	5.2.3
NIR CC (4Aug)	LAI_{AZ} (4Aug)	0.017	1.864	-0.636	0.279	5.2.4
NIR CC (9Aug)	LAI_{AZ} (9Aug)	0.005	2.039	0.030	0.232	5.2.4
NIR CC (12Aug)	LAI_{AZ} (12Aug)	0.016	1.787	-0.207	0.276	5.2.4
NIR CC (16Aug)	LAI_{AZ} (16Aug)	0.010	1.705	-0.056	0.194	5.2.4
NIR CC (25Aug)	LAI_{AZ} (25Aug)	0.006	1.705	0.122	0.177	5.2.4
NIR CC & Date	LAI_{AZ}	0.012 & -0.025	2.078	0.582	0.261	5.2.4
NIR CC & GDD	LAI_{AZ}	0.012 & -0.002	3.441	0.579	0.262	5.2.4
NIR CC & Date (AAC Magnet, AAC Prevail, and Carberry are excluded)	LAI_{AZ} (AAC Magnet, AAC Prevail, and Carberry are excluded)	0.014 & -0.024	2.030	0.632	0.228	5.3
NIR CC & Date (First Cluster)	LAI_{AZ} (First Cluster)	0.012 & -0.023	2.033	0.586	0.231	5.3
NIR CC & Date (Second Cluster)	LAI_{AZ} (Second Cluster)	0.018 & -0.033	2.172	0.834	0.188	5.3
NIR CC (Cropped)	LAI_{AZ} (Cropped)	0.022	1.512	0.505	0.285	5.3
NIR CC & Date (Cropped)	LAI_{AZ} (Cropped)	0.012 & -0.024	2.045	0.591	0.258	5.3
NIR CC & Date (First Cluster-Cropped)	LAI_{AZ} (First Cluster-Cropped)	0.011 & -0.023	2.219	0.585	0.232	5.3
NIR CC & Date (Second Cluster-Cropped)	LAI_{AZ} (Second Cluster-Cropped)	0.023 & -0.027	2.043	0.804	0.229	5.3